UNIVERSITY OF THE WITWATERSRAND
JOHANNESBURG

School of Physics

The culprit for the termination of Mars' magnetic field: Dark Matter

---

Student Name: Javeria Makda
Student Number: 1814764
Supervisor: Dr. G. Beck

A dissertation submitted to the Faculty of Science of University of the Witwatersrand, Johannesburg, in fulfilment of the requirements for the degree of Masters in Science.

Abstract

The reason for a significant change in the heat flux of the interior of Mars, leading to the termination of its magnetic dynamo, is not yet known. We present the idea that interaction of dark matter particles with the elements constituting the core of Mars is the cause for this significant heat flux change. We include resonant enhancements in the determining of the capture rate of dark matter particles by a planet, using more recent formulations. The exclusion limits for the interaction cross-sections in our work are more stringent than previous limits. We demonstrate, using Xenon1T limits, that the density of dark matter in our solar neighbourhood is insufficient to induce significant heating. However, encounters with low-mass ultra-compact mini-halos or very massive conventional sub-halos could both produce significant heating effects within terrestrial planets. We find that in 1 Gyr, there is a possibility of up to ~ 860 interactions of Mars with an ultra-compact mini-halo, that would have the sufficient density and mass to alter the workings of the convective core of Mars, such that it would lead to the cessation of the Martian geodynamo. The interaction of Earth with these halos would not result in the cessation of its magnetic field due to mechanisms such as tectonic activity, crust recycling and the subsequent motion of molten iron in its outer core, which result in the continuous functioning of the geodynamo.

Declaration

I declare that this dissertation is my own, unaided work. It is being submitted for the Degree of Master of Science at the University of the Witwatersrand, Johannesburg. It has not been submitted before for any degree or examination at any other University.

Signed: ____________________

Date: 28/05/2024

Acknowledgements

We would like to acknowledge the NRF for funding this research through its post-graduate bursary initiative.

Contents

Contents

1. Introduction

Due to magnetic remnants in some rocks on Mars [1, 2], research has confirmed that there was once a global magnetic field for Mars much like the one Earth has. This is believed to have been powered by a core convection dynamo mechanism. It has not yet been confirmed as to what switched off this geodynamo and led to the termination of this magnetic field. There is a consensus that a significant change in the heat flux of the interior of Mars could lead to the termination of this geodynamo [3, 4, 5]. There are several studies exploring potential causes for the termination of Mars' magnetic field [4, 6, 7, 8, 9], such as additional energy from extra-martian impacts, the end of tectonic activity on Mars, magmatic degassing of the mantle or a gradual decrease in core temperature. None have mentioned dark matter as the cause.

In 1985, Press and Spergel [10] hypothesized that a population of weakly interacting massive particle (WIMPS) present in the sun could solve the solar neutrino problem and that these particles could also make up the absent mass in the galaxy. In doing so, they calculated the number of these particles that would've been scattered and subsequently remained in bound orbits around the sun. They deduced the probability that a scattering event would occur, and the probability that a scattering would lead to the WIMP being gravitationally captured. It was concluded here that there exists a narrow but feasible parameter range for which a Galactic population of stable WIMPs could resolve the issue of the absent mass in the Galaxy as well as the solar neutrino problem via capture. Shortly after that, Gould [11] derived the precise formulation for the capture rate of WIMPs by a massive body e.g the Earth or Sun. The limits for the disruption of capture and annihilation, such as effects from the Moon, were accounted for. The interaction cross-section formulation developed in this study considered both the mass of the element scattering the WIMP, and the mass of the WIMP itself. It was further found here that, if an element is abundant in the Earth, the capture rate of WIMPs which have a similar mass to the nuclear mass of this element is notably increased. Works relating mass extinctions and period volcanic activity on terrestrial planets, to dark matter have shown that sufficient capture and annihilation of dark matter particles can influence the flow of heat in the planet [12, 13]. Most recently, Leane and Smirnov [14] have presented exoplanets as new probes to discover dark matter. It was noted that a dark matter origin could be spotted using the correlation between galactic position and dark matter-induced heating in exoplanets, as this would provide an idea of the dark matter density. Two searches were suggested: one for overheated local exoplanets, and the other, for overheated exoplanets correlated with dark-matter density, spiking in temperature towards our galactic centre.

Here, we present interaction with dark matter particles, specifically weakly interacting massive particles (WIMPs) as a possible source of change in the heat flux of Mars' interior, and thus the potential cause behind the cessation of Mars' magnetic field. We suggest that the heat from dark matter annihilations leads to the degassing of the mantle, as described by Sandu and Kiefer in Ref. [9]. We explore previous values for the rate of acquisition of dark matter particles, and the subsequent heat production from dark matter-dark anti-matter annihilations. This is then compared to much more recent formulations and observations, where we incorporated the addition of resonant effects. After finding the most sensible approach, we proceed with calculating how dense a clump of dark matter would need to be in order to cease the convection in the interior of Mars. We lastly find how likely an encounter with such a clump would be in a given timeframe so as to give an idea of how high the probability is of our hypothesis being correct.

In this section, we introduce the problem we intend to study and the scientific motivation for that. Additionally, we briefly provide the context of this work in terms of the observations and conclusions seen from previous studies based around this topic. In chapter 2, a background on dark matter is provided. We discuss what it may or may not be, the reason it is postulated to exist, current research and methods on its detection, and potential density profiles. In chapter 3, the link to heat injection in terrestrial planets is presented. We discuss work done in the past regarding dark matter capture and heat injection on Earth, present the history of Mars' magnetic field and internal dynamo, and some of the other hypotheses for the cause of the termination of the martian geodynamo. In section 4, we present the formulae, data and analyses used to achieve our results. Our assumptions, steps and results produced can be found in this section. Lastly, we provide a brief summary of our method and findings.

2. Dark Matter

2.1. What is dark matter?

Dark matter, named appropriately as such, is a type of hypothetical non-luminous matter that is postulated to exist. It constitutes majority of the matter in the universe (∼85%). It is believed to be comprised of non-baryonic (a type of matter that is not composed of baryons) particles due to the fact that it does not associate with the electromagnetic field, meaning that is most likely is not the normal stars, interstellar clouds and planets we see. The only way that baryonic matter could possibly be a major constituent of dark matter is if it was all bound in brown dwarfs or in massive compact halo objects (MACHOs), which are small, dense clumps of heavy elements [15].The other options of galaxy-scale black holes and antimatter have also been mostly ruled out as being dark matter through observations and calculations [16].

2.2. Evidence for its existence

The reason it is so strongly believed that this non-luminous matter exists is due to many theoretical and experimental motivations. One of the first emergences of the idea of dark matter is seen in the study of the Coma cluster performed by Zwicky [17]. In order to explain the significant amount of dispersion observed in the velocities of the galaxies in the the Coma Cluster, he applied the virial theorem and found that the density and subsequent mass of the cluster is far greater than what is found from luminous matter alone. This implied that not only was there missing matter, but that it is much greater in abundance than luminous matter. Furthermore, it was found that if the average density was assumed to be solely due to luminous matter, then whether the cluster was or was not in stationary equilibrium, the cluster would break apart due to the enormous observed speeds. That is clearly not the case. Even if the speeds were seen as being caused by gravitational or cosmological redshift, the conclusion still remained that a great density of dark matter was required. After Zwicky, many observations of the rotation curves of galaxies were made and exhibited a characteristic plateau at large distances [18]. One such study of note is Babcock's of the Andromeda galaxy [19].

Einstein's theory of general relativity predicts the occurrence of gravitational lensing. This is a phenomenon where incoming radiation from a background source is bent by a massive object on its journey to Earth as a consequence of the warping of space-time in the massive object's gravitational field, in the foreground. The consequences of this are multiple images of the background object, giant arcs or complete rings (known as Einstein rings) around the foreground object, or minor distortions in the shape of the background source. This is something that allows for the determination of dark matter content or distribution in galaxies and galaxy clusters. A study of an early-type lens galaxy in the system 0047-281 by Koopmans and Tommaso [20] found that the mass-to-light ratio calculated by analysing the deviation from the local fundamental plane characteristics, is insufficient to explain the mass measured within the Einstein radius. Furthermore, X-ray observations found an atmosphere of hot gas within the dark halos around the elliptical galaxies. The pressure of the gas balances the gravitational attraction of the dark matter, preventing the gas from collapsing further. This, in turn, implies the presence of additional unseen mass (dark matter) in the dark halos of these galaxies, which provides the necessary gravitational force to support the gas. Further work done on constraining dark matter and its substructure using strong and weak gravitational lensing using various other sources can be found here [21, 22, 23].

The rationale used by Oort was applied in the findings of a survey of K-giants [24] to provide evidence for disk dark matter in the Milky Way. When considering the amount of K-stars that were found in the southern galactic pole, the gravitational potential implied by their distribution was not feasible with a model where there was no dark matter. The data is only compatible with a model which has a dark matter distribution comparable to that of normal matter. It was also found here that the best-fit model had 53 % more dark matter than luminous matter.

Although the cosmic microwave background (CMB) is nearly uniform, the minor temperature fluctuations observed in its spectrum are significant in pushing forth the idea of dark matter. These anisotropies in the CMB reveal density variations in the universe when it was young, which provided the foundation for the development of galaxies and large-scale structures we see today. These small density perturbations were enhanced by gravity in order to produce the distribution of mass in the current state of the universe. If only visible matter is considered to provide all the mass in the universe, the observed fluctuations in the CMB would not be sufficient to explain the present-day structures. Visible matter alone does not provide enough gravitational attraction to elucidate the observed distribution of galaxies and galaxy clusters. Thus, dark matter is postulated to be the missing ingredient that provides the additional gravitational attraction needed to account for the observed large-scale structure of the universe. A study done by Peebles [25] of the large scale background temperature and mass fluctuations assumed a model where the universe is dominated by WIMPs. This was one of the first studies to show that models that include non-luminous matter fit the observations well and can therefore contribute to the improvement of the framework of cosmology.

Some additional proof for the existence of dark matter was found during studies of the velocity dispersions of dwarf spheroidal galaxies and spiral galaxy satellites where the mass-to-light was calculated to be larger than that previously observed [26].This also led to the inference of dark matter halos surrounding spiral galaxies.

2.3. What could make up dark matter?

As mentioned above, there is much more certainty about what it is not than what it is. It is most commonly believed that dark matter is comprises of axions or weakly interacting massive particles (WIMPS). The general characteristics of WIMPs are that they are electrically neutral, interact with standard model particles on the Weak or Sub-weak scale, have features of non-baryonic matter, and their self-interaction strength is not extremely high so that there is not any conflict with limits on structure formation [27]. Some hypothetical particles that are thought to possibly make up these WIMPS are provided by frameworks such as the Twin Higgs Mechanism,the Little Higgs Model, Kaluza-Klein States and Supersymmetry [28, 29], where some of the proposed dark matter candidates are the supersymmetric partner of the neutrino (sneutrino), which could be a type of non-thermal WIMP, the neutralino and the gravitino. The leading candidate for what WIMPs could be are neutralinos, which are hypothetical particles which are far more massive and slower than neutrinos but interact with ordinary matter quite weakly making them difficult to detect. Neutralinos are composite particles formed as a combination of the Z boson, the supersymmetric partners of the photon, and both neutral CP-even Higgs bosons found in the minimal extension of the supersymmetric standard model [30, 28].

When considering non-WIMP dark matter candidates, one of the most favoured are axions. Quantum chromodynamics is the fundamental gauge theory that describes the behaviour of the strong nuclear force. It was noted that a theoretical term in this description allows for the violation of the combined symmetries of charge conjugation and parity, known as the CP violation in particle physics. In an attempt to solve this, a global symmetry was introduced by Peccei and Quinn that spontaneously breaks at low energies and results in the axion [28]. It has been seen from laboratory searches, stellar cooling and supernovae data, that axions would be extremely light particles [29]. This means that their interactions with ordinary matter would be extremely weak and as a consequence, they would never have been in thermal equilibrium in the early universe. If the primary theory here is supersymmetry, then there should additionally exist a supersymmetric partner for the axion i.e. the axino. Axions and axinos, if they exist, form part of Cold dark matter - a type of dark matter composed of particles with little kinetic energy that would be gravitationally attracted to each other and form structures by clumping together.

Similar to the prediction of axinos, another possible cold dark matter candidate hypothesized by supersymmetry is the gravitino. This is the supersymmetric partner of the Graviton which is a hypothetical particle that mediates the force of gravitational attraction. In some models, these can be the lightest supersymmetric particle and are also stable [26], thus making excellent dark matter contenders.

Another interesting hypothetical particle put forward as dark matter is the sterile neutrino. Sterile neutrinos are hypothetical particles that emerge in the extension of the Standard Model and were introduced to explain neutrino oscillation phenomena, where neutrinos change from one flavour to another. These particles (sterile neutrinos) are believed to not interact through the Weak interaction, but rather through fermion mixing [29]. Constraints have been put on sterile neutrinos by examining their cosmological abundance as well as studying their decay products. Surveys such as WMAP have found that for sterile neutrinos to make up dark matter, they cannot have masses lower than 10 KeV [26].

Some alternative dark matter types that are worth noting are Wimpzillas: hypothetical dark matter particles that are too massive to be produced through thermal processes in the early universe because their masses exceed the reheating temperature after inflation; pseudo Nambu-Goldstone bosons; SIMPs (strongly interacting massive particles) arising from certain supersymmetric models; gauge theories with exotic stable heavy quarks; and primordial black holes [31].

2.4. Detection techniques and current experiments

There are three main types of approaches when considering how to detect dark matter. The first is direct detection: the consequences of dark matter particles interacting or colliding with ordinary matter (usually the material in the detector) such as nuclear recoil or energy and momentum transfer, are measured and allow for the inference of dark matter properties. Some ways that this nuclear recoil energy is measured are by inspecting scintillation, photons and ionization. The calculations here require the WIMP-nucleon scattering cross-section as well the local density and velocity distribution of the WIMPs [26]. The detectors are usually large and placed deep underground in order to prevent any background sources such as cosmic rays colliding with the nuclei of the detection material. The most common types of direct detection experiments use solid-state (e.g. CDMS in Soudan Underground Laboratory), liquid (e.g. Xenon1T at Gran Sasso in Italy), cryogenic (e.g. EDELWEISS in France) or scintillation detectors (e.g. NaI(Tl) crystal experiment in Y2L underground facility) [32]. The results from the search for axion-like particles and dark photons by the SuperCDMS experiment can be seen in Figure 1. In 2020, the first germanium-based constraints on sub-MeV dark matter particles, as well as dark photons down to 1 eV, were obtained by the EDELWEISS experiment as seen in Figure 2. The study set new limits on the kinetic mixing of dark photon dark matter in an unconstrained parameter space region, demonstrating the high relevance of cryogenic germanium detectors in dark matter searches.

The second is indirect detection: the products from dark matter and dark anti-matter annihilations and the decay of dark matter particles are detected. The most common signals searched for in this scenario are gamma rays, neutrinos, or cosmic rays. The ideal locations for searching for these products are areas which are believed to have a high density of dark matter, such as the Galactic center. dark matter annihilation can also be boosted by heavy astrophysical bodies such as the Sun; these objects can slow down and capture the dark matter particles and therefore increase the rate of annihilation. An additional way of indirectly detecting dark matter is through the analysis of synchrotron radiation that would be emitted by secondary electrons and positrons (produced by the decay or self-annihilation of dark matter) travelling through the galactic magnetic fields [26]. The most well-known system for indirect detection of dark matter is the CTA (Cherenkov telescope array) observatory currently located in Chile. Recent results from this and the IceCube DeepCore collaboration can be found in Figure 3 and Figure

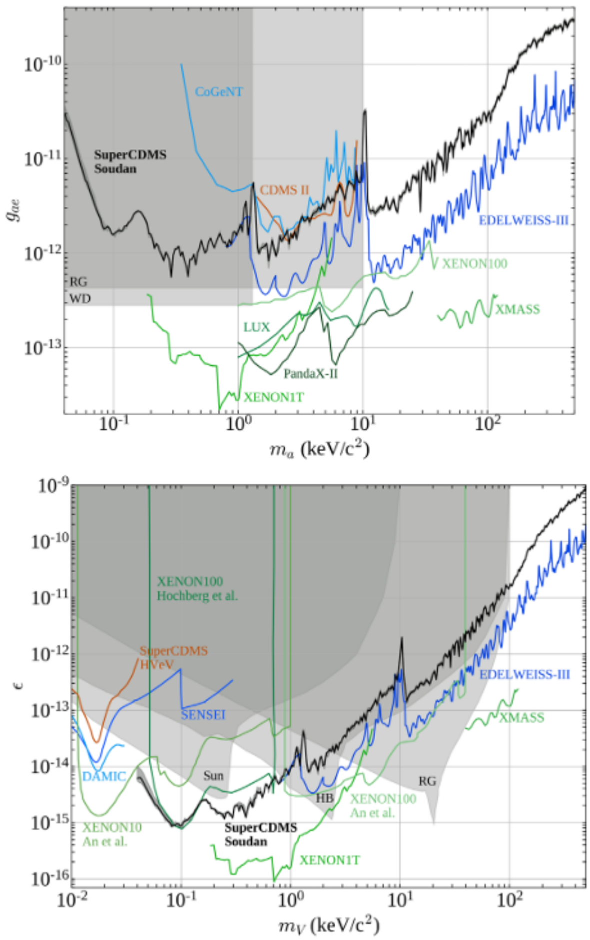

Figure 1 : Exclusion limits on the axioelectric coupling g_{ae} and the dark photon mixing parameter ϵ (solid black line) obtained as results by the SuperCDMS Underground Laboratory [33]. The shaded grey area represents the uncertainty band. Limits from other direct-detection experiments are also shown.

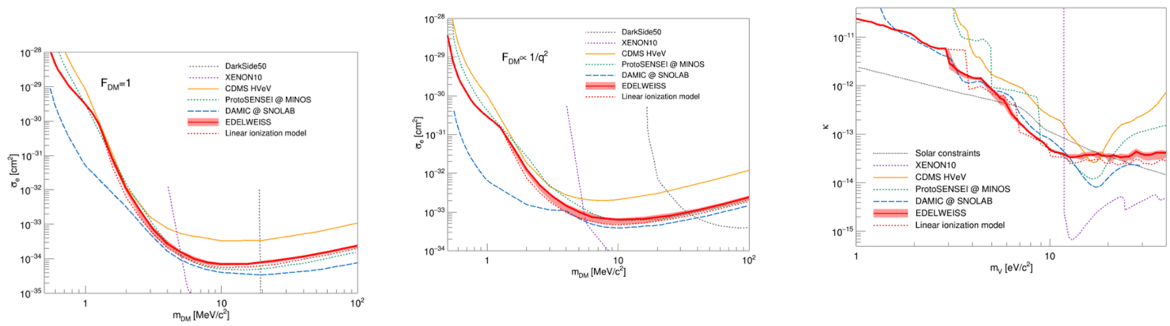

(a) (b) (c)

Figure 2 : Upper limits on the interaction cross-section for dark matter particles and electrons, assuming a heavy mediator first, and then a light mediator, as obtained by [34]. Image (c) shows the upper limits obtained for the kinetic mixing κ of a dark photon. The limits found by other direct-detection experiments are additionally shown.

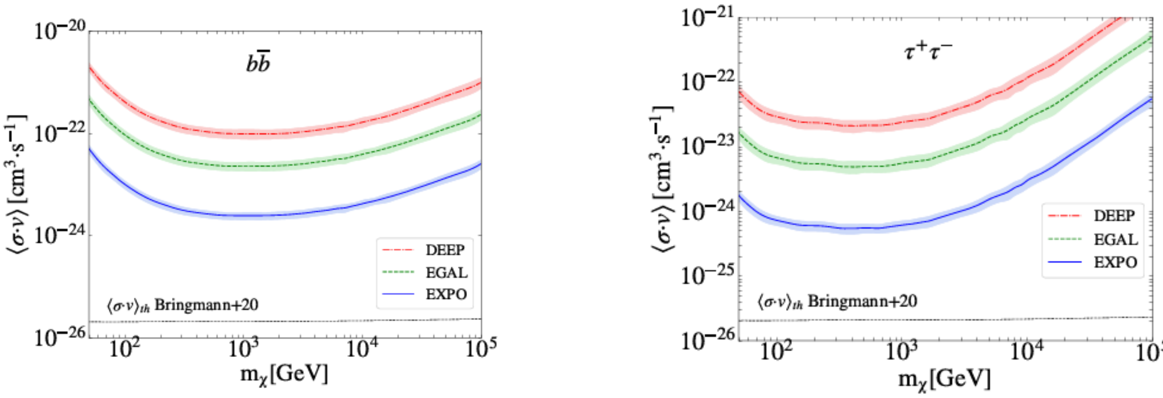

(a) (b)

Figure 3 : Upper limits found at a 95% confidence level by CTA [35], to the dark matter annihilation cross-sections for a $b\bar{b}$ (left) and $\tau^+\tau_-$ (right) annihilation channel. The shaded area represents the uncertainty arising from the minimum flux required for detection.

4 respectively. In the results produced by CTA [35], the detectability of dark sub-halos was examined using three different observational scenarios (EGAL, DEEP, EXPO) and constraints on the dark matter self-annihilation cross-sections were found under the assumption that no dark sub-halo is detected by CTA. The limits placed on the dark matter annihilation cross-sections by IceCube [36] used five years of data to examine dark matter particle masses ranging from 10 GeV to 40 TeV. This is the first devoted search with a neutrino telescope. Furthermore, the lower limits for the lifetimes of decaying dark matter were also derived in this analysis.

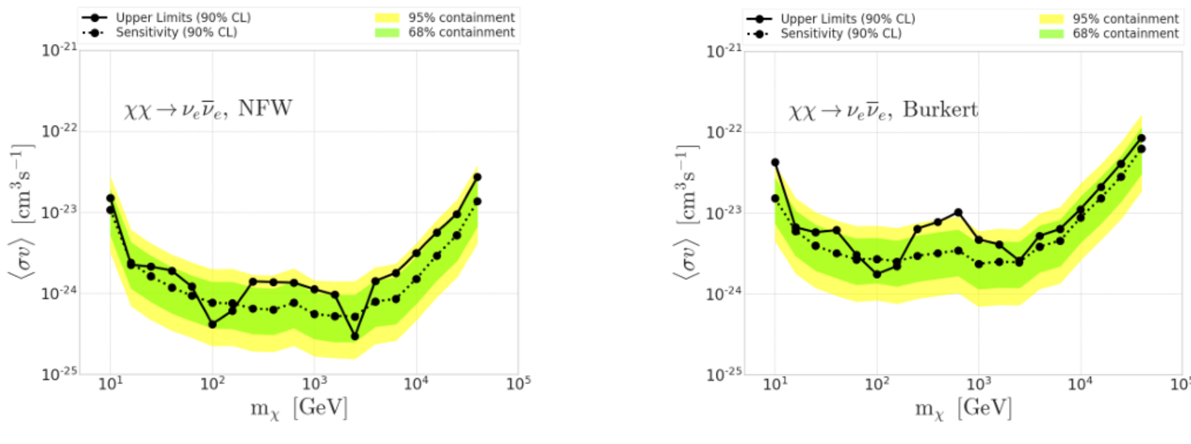

(a) (b)

Figure 4 : Upper limits found at a 90% confidence level by the IceCube DeepCore collaboration [36], for the thermally averaged dark matter self-annihilation cross-sections considering two dark matter profiles: NFW (left) and Burkert (right). See section 2.5 for details of dark matter profiles.

The last method is using a particle collider, the most well known being the Large Hadron Collider (LHC). The investigation into dark matter at the LHC is predicated on the hypothesis that Standard Model particles can interact or in certain cases decay into dark matter particles.

By colliding high-energy protons and studying the energy and mass of the products, the LHC can search for signals of dark matter. This can be done by looking for any missing momentum or energy in the detector post-collision, which could have escaped as dark matter due to it interacting extremely weakly with other matter. Additionally, studying any mediator particles that may be produced by these collisions, which would decay into standard model particles, allows for the comprehension of the characteristics of dark matter particles. A summary of dark matter searches at a centre of mass energy of 13 TeV from the ATLAS collaboration is presented in Ref.[37]. These focused on mono-X signatures where "X" represents a visible particle produced alongside a dark matter particle, and recoils against the missing transverse momentum vector. These visible particles could be things like jets (sprays of particles), photons, or electroweak bosons (particles responsible for the weak nuclear force). In certain theoretical models beyond the Standard Model of particle physics, there are interactions proposed between dark matter particles and the Higgs boson. These interactions allow for the production of dark matter particles in association with a Higgs boson. The Higgs boson can decay into various particles, such as a pair of photons, a pair of bottom quarks, or a pair of Z bosons. The mono-Higgs search at ATLAS looks for dark matter production for al three decay channels. Since no evidence of dark matter has been observed in these searches, the results, as can be seen in Figure 5 are given in the form of excluded regions from the mono-jet and mono-photon searches and compared with dijet resonance constraints. Dijet searches look for the existence of new particles that decay into a pair of jets with specific characteristics. While the experiment has not yet directly detected dark matter, it plays a critical role in constraining theoretical models and exploring energy regimes where new particles, including potential dark matter candidates, might exist.

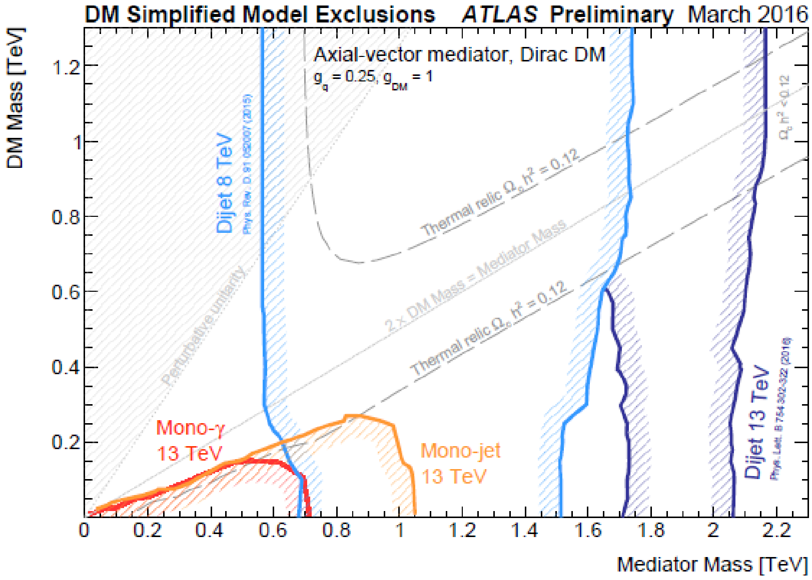

Figure 5 : ATLAS mono-jet, mono-photon, and dijet exclusion limits as a function of dark matter mass and mediator mass in the framework of simplified models with an axial vector mediator [37].

2.5. Dark matter profiles

In order to place limits on cross-sections for dark matter annihilation and dark and normal matter collisions, it is vital to know the density and velocity distribution of dark matter around us. Dark matter profiles refer to the distribution or density of dark matter as a function of distance from the center of a celestial object, such as a galaxy or a galaxy cluster. These allow us to comprehend how dark matter is distributed within these structures and are imperative for understanding the gravitational effects of dark matter on luminous matter. The shape and mathematical form of these profiles depend on which model they are based on and what assumptions were made. Although there is general agreement regarding the average density distribution of dark matter at large distances, there is still dispute regarding the form of the profiles in the core of galaxies and clusters [26]. The most widely known models are the NFW, Einasto, Burket, and Moore profiles.

In 1995, Navarro, Frenk and White studied the forms of dark halos of dwarf galaxies and rich galaxy clusters using N-body simulations [38]. They first found the spherically averaged density for dark matter halos as

$$\rho(r) \propto \frac{1}{r(1+\frac{r}{r_s})^2} \tag{1}$$

where ρ(r) represents the density of dark matter at a given distance from the center of the halo r, and r_s is a characteristic radius that determines the scale of the halo. This profile can be scaled to fit the density profiles of halos with a wide range of masses. They then selected halos with a wide range of masses obtained from previous cosmological simulations of large regions of interest and then resimulated each of these halos individually at a much higher resolution. For the N-body simulations, the softening length and virial radius of each halo was considered and the masses used ranged from halo-masses of dwarf galaxies all the way to halo-masses of galaxy clusters. This then led to the modification of the equation above to produce this model:

$$\frac{\rho(r)}{\rho_{crit}} = \frac{\delta_c}{(\frac{r}{r_s})(1+\frac{r}{r_s})^2} \tag{2}$$

where ρ_{crit} is the average density needed to halt the expansion of a flat universe (depending on the present value of Hubble's constant), δ_{c} represents the characteristic overdensity of the halo indicating the extent to which the halo's density exceeds the average density of the universe at that particular time, and r_s (scale radius) reflects how quickly the density profile falls off with distance. This density distribution increases rapidly towards the center and falls off slowly at significant distances from the center. This was later extended to give the Generalized NFW Profile [39]:

$$\rho(r) = \frac{\rho_s}{\left(1+\left(\frac{r}{r_s}\right)^{\alpha}\right)^{\left(\frac{\beta-\gamma}{\alpha}\right)}\left(\frac{r}{r_s}\right)^{\gamma}} \tag{3}$$

where ρ_{s} is the characteristic density and α, β and γ are parameters used to manipulate the shape of the profile. It includes additional parameters to account for more complexity and is often used to fit observations from X-ray and Sunyaev-Zel'dovich effect data. This makes it more flexible to fit to observations. Moore et al. [40] conducted a number of N-body simulations to model Cold dark matter halos, comparing these models to the observed rotation curves of dwarf galaxies and galaxies with low surface brightness. Their work aimed to show that the Cold dark matter dominated universe does not align with the rotational behaviour of galaxies primarily consisting of dark matter. Using the GNFW profile's form, they found the data to be best fit by assuming a region with uniform density at its center i.e. $\alpha = 2, \beta = 3, \gamma = 0$.

In contrast to the cuspy profiles predicted by NFW, the Burkert profile [41] predicts a cored dark matter density profile. It is an empirical model which focuses on describing the density distributions in dwarf and low-surface brightness galaxies. The Burkert profile has the following form:

$$\rho(r) = \frac{\rho_0}{(1+(\frac{r}{r_s})^2)(1+\frac{r}{r_s})} \tag{4}$$

where ρ_0 is the density at the center.

In a paper focusing on forming a composite model for the galaxy in addition to studying the influence of galactic parameters by Einasto [42], another mathematical model was introduced regarding the density arrangement of dark matter halos. This model had the form:

$$\rho(r) = \rho_0 \exp\left(\frac{-2}{\alpha}\left[\left(\frac{r}{r_s}\right)^{\alpha} - 1\right]\right) \tag{5}$$

where α is a shape parameter that determines the steepness of the density profile. Unlike the NFW profile, the Einasto profile is more flexible and can be used to study a broader range of dark matter distributions. This profile is more applicable when considering the outer regions of dark matter halos.

Although there is no consensus regarding which galaxy types are described by which dark matter profiles, there are some interesting studies which explore this. A recent study of the Milky Way performed by Xiaowei et al. provided an updated model of the dark matter distribution in our galaxy, by constructing the circular velocity curve from the center to a distance of 30 kpc [43]. Compared to the inner parts of the galaxy, it was discovered here that there is a significantly faster decline in the velocity curve at outer galactic radii. It was found that the decline was better described by a cored Einasto profile in comparison to a Generalized NFW profile. Additionally, it was noted that the virial mass calculated using the Einasto profile is significantly lower than the mass obtained from the Generalized NFW profile. An older study by Gentile et al. [44] examined the H1 data and the Ha rotation curves of five spiral galaxies to deduce the distribution of dark matter therein. H1 data refers to observations of neutral atomic hydrogen emission in the form of radio waves at a wavelength of 21 centimeters. Ha rotation curves are the rotation curves derived from observations of hydrogen-alpha emission in galaxies, which often arises from regions of ionized hydrogen gas associated with star formation activity. The density distribution was compared with various distributions such as the Moore profile, Burkert profile, and NFW profile. It was noted here that both the Moore and NFW profiles could not accurately describe the dark matter halos that are surrounding the galaxies in the sample. The conclusion from the study of these galaxies was that the Burkert profile best fit the rotational velocity curves obtained, with no systematic deviations, thus these galaxies are uniquely fitted by cored haloes. The dark matter distribution of elliptical galaxies is even more scarcely studied as compared to spiral galaxies. Using a joint lensing-dynamics approach, the internal structure of 23 galaxies was investigated [45]. It was concluded in this research that the dark matter haloes of the elliptical galaxies considered in the study are best described by the NFW profile.

The aforementioned profiles all result in roughly the same density at significant distances away from the central region of the halo. The work done here is limited to our solar system, particularly the region around Mars and Earth. Thus, regardless of the profile chosen, the value used in calculations for dark matter density and distribution remained constant.

3. Magnetic fields of Earth and Mars

3.1. History of Mars

Mars was formed around 4.6 billion years ago with the rest of the planets in our solar system. There are two main theories for the explanation of how Mars formed: the core accretion model and the disk instability model [46]. The core accretion model puts forward that giant planets formed through the initial accretion of dust and ice to form a solid core. The small clumps of solid particles that joined together are referred to as planetesimals which are the seedlings for asteroids, comets, moons and planets. According to this hypothesis, the force of the solar wind was responsible for clearing away lighter elements like hydrogen and helium from the inner areas of the solar system, resulting in the formation of primarily small, terrestrial planets. Conversely, in the outer parts of the system, the influence of the solar wind diminished. Once the mass of the core attains a critical value, it can attract gas from the surrounding protoplanetary disk to form a massive atmosphere, evolving into a gas giant. On the other hand, the disk instability model suggests that the swift formation of giant planets occurs through the gravitational collapse of a substantial, confined area of dust and gas. This dense agglomeration within the protoplanetary disk succumbs to its own gravity, creating a giant planet directly without requiring a pre-existing solid core. This concept emerged to account for the necessity of gas giants to form quickly to capture their extensive envelopes of lighter gases — a phenomenon that the core accretion model struggled to justify in simulations. Core accretion is generally considered a slower process compared to disk instability. The gradual accumulation of solid material to form a core, followed by gas accretion, takes a longer time, often millions of years. Furthermore, the disk instability model suggests that planets obtain orbit-stabilising masses much quicker so that they do not spiral into the Sun. Both models suggest that Mars should be far more massive than it is, approximately the same as Venus and Earth. The leading theory to give grounds for this discrepancy is the Grand Tack model [47]. This suggests that Jupiter and Saturn moved closer towards the Sun shortly after their formation, due to interactions with the gas and dust present in the protoplanetary disk. Since Jupiter had a larger mass, it moved faster. Due to this inward migration, they reached an orbital resonance which caused them to shift their migration directions. According to the model, during Jupiter's outward migration, it disrupted the formation of Mars by taking with it much of the matter that would have contributed to the make up of the planet. An alternative idea put forward is that Mars had initially formed at the location of the asteroid belt and then migrated inwards because of its interaction with planetesimals, which would cause it to lose energy [46]. Similar to Earth, Mars underwent differentiation. This was due to the planet's temperature from the energy from all the collisions. It separated into distinct layers, with the densest elements forming the core, a silicate mantle, and a crust made of the least dense silicates. This process also released heat, which contributed to Mars' early geological activity.

While studying the accretion process of Asteroid 6 Hebe and the thermal effects thereof, it was noted that it is necessary to consider the effects of early accretion on the thermal evolution of Mars and other planetesimals [48]. The purpose of this was to improve thermal evolution models so that questions relating to the thermal processes of Mars in the past, can better be addressed. This information would allow valuable insight into the separation of the different layers of Mars as well as the formation of interesting regions such as the large volcanic plateau Tharsis.

Some of the initially developed early thermal evolution models for Mars assumed that shortly after its formation and accretion, the planet started out with relatively low temperatures. The accretion models referenced offered an estimated timeframe for accretion ranging from 100 to 1500 million years. In contrast, dynamic models indicated that substantial heating from large impacts occurred during this accretion process [49], which led to the development of models that depict Mars as initially hot. The majority of thermal evolution models used a value of accretion time around 100 Myrs (Megayears), meaning that only heating by long-lived radionuclides was considered [48]. These were then improved upon by accounting for the heat from impacts and from core formation. Contrary to what was initially widely believed, some accretion models have demonstrated a much shorter timescale for accretion i.e. $\sim$ Myrs. This was done by considering the idea of runaway growth which is a phase in the process of planet formation where solid particles, such as dust and small rocks, begin to rapidly accumulate and grow into larger bodies, ultimately forming planetesimals and then planetary embryos. This rapid accumulation is due to the dominance of some planetesimals within their local region which result in them having a greater gravitational pull and thus obtaining a larger size in a shorter time interval. The theory suggests that Mars could be a remaining planetary embryo, resulting from a process of rapid accretion and differentiation. This model gains support from various sets of isotopic evidence. Specifically, the hafnium-tungsten isotopic system, a method for isotopic dating, has been used to show that Mars underwent complete accretion, differentiation, and silicate melting within approximately 10 million years in relation to the formation of calcium-aluminum-rich inclusions [48], which are some of the solar system's oldest and first-formed solid materials.

For the purpose of analysing the effects of accretion on the early thermal evolution of Mars, Ghosh et al. [48] makes use of two models. One of these assumes an undifferentiated planet during the accretion process, while the other starts with a planet that is already differentiated into a core and a mantle. A key distinction between the two theories is that while the initial model applies a gradual accretion and thermal model without considering the separation between the planet's core and crust, the alternative approach revisits the influence of radioactive aluminum ($^{26}_{13}$Al) in a context where Mars accreted quickly. In this latter model, the calculations take into account not only heat from impact events but also from early tectonic processes. It has been observed that Mars' swift formation emphasizes the potential impact that $^{26}_{13}$Al could have on Mars' early heat history. Indeed, the heat output of $^{26}_{13}$Al per unit mass and time surpassed that of all other radioactive sources combined in the first 5 million years following the creation of calcium-aluminum-rich inclusions. The fast accretion of Mars allows for a shorter timescale for the presence of $^{26}_{13}$Al, which contributes significantly to the early thermal evolution of the planet. The differentiation and thermal history of Mars are impacted by the enhanced heating caused by the presence of $^{26}_{13}Al$ in the early phases of the planet's thermal evolution. When $^{26}_{13}Al$ was present, in particular, the redistribution of radionuclides during differentiation might have led to non-uniform heating of Mars' crust and mantle. Consequently, following core formation, $^{26}_{13}Al$ and $^{60}_{26}Fe$ would separate into the mantle and core, respectively. This would raise the mantle's temperature well above that of the underlying core and have an additional impact on Mars' thermal history.

Mars' early thermochemical condition and rheology are major factors in its capacity for deformation and dynamic evolution. Samuel et al. [3] examined the orbital development of Phobos, the nearest and largest moon of Mars, to get additional insight into the rheology and temperature history of the planet. This is due to the fact that through tidal interactions, Mars' thermochemical history controls the orbital evolution. Mars experiences a tidal bulge due to Phobos's deforming gravitational pull. Surface observations, thermal and magnetic constraints (to comprehend the relationship between the thermal state and mantle rheology of Mars), the degree-two Love number (k2) and tidal quality factor (Q) of Mars were some of the other constraints that were used in this study. Mars' response to tidal forcing is characterized by the degree-two Love number, which is only marginally sensitive to temperature. The tidal quality factor, which is highly temperature-dependent, quantifies tidal dissipation on Mars. This study explored the long-term evolution of the three primary layers that Mars comprises of: the evolving lithospheric lid, which contains a crust rich in radiogenic materials, the homogeneous silicate convecting mantle, and the liquid metallic core. With these considerations taken into account, an average surface heat flow of 20 ± 1 milliwatts per square meter was estimated for Mars, and a current average crustal thickness of 40 ± 25 kilometres. Once the additional effect of an early surface ocean was taken into account for the model, the predicted value for crustal thickness went down to 33 km $\pm$ 2 km. It is proposed here that Mars was moderately hotter in its early life post-formation and its mantle deforms extremely slowly through the movement of dislocations in the material, which are line defects in the crystal lattice structure. This allows for deformation without fracturing. This indicates a moderate to relatively weak intrinsic sensitivity of viscosity to temperature and pressure. This deformation in the mantle has a corresponding intrinsic activation energy of 280 ± 80 kJ/mol and an activation volume less than 14 cm^3/mol [3]. However, when an early surface ocean was taken into consideration, the intrinsic activation energy value decreased to 220 ± 15 kJ/mol. The intrinsic activation energy is associated with the breaking and forming of chemical bonds or the overcoming of other barriers that hinder the progress of the deformation in the dislocation creep regime. Intrinsic activation volume is the change in volume associated with process.

To explore the internal dynamics and thermal evolution of Mars, researchers have developed sophisticated models and computational methods [50, 51]. These models cover a range of phenomena including surface heat distribution, seismic activity, impacts, differentiation between the crust and mantle, and the evolution of the magnetic field. A recent study in 2022 by Plesa et al. [52] reviewed 3D global geodynamic models in light of data from the InSight mission, aiming to refine parameters like mantle viscosity, distribution of heat flow, and heat exchange at the core-mantle boundary. This enhances our understanding of Mars' thermal history and its current state. Key findings from this study indicate that surface heat distribution, the pattern of elastic lithospheric thickness, and the location of mantle melting zones are significantly influenced by variations in crustal thickness. Moreover, it suggests that the temperature of the lithosphere and seismic velocities in the narrow layer between the lower mantle and the outer core, mirror the thickness pattern of the crust. The study suggests that mantle convection may occur on a smaller scale than previously assumed due to the large size of Mars' core. The concept of thermal lithospheric thickness, representing the depth where temperatures reach a critical threshold, is crucial. Mars' average thermal lithospheric thickness, estimated at 400-600 km, suggests substantial cooling over its thermal history [52]. This thick lithosphere contributes to the formation of low-velocity zones within Mars' interior. To refine thermal evolution models for Mars, the study proposes considering seismicity distribution, Chandler Wobble effects, and seismic wave propagation. These factors can provide insights into the tidal quality factor, mantle viscosity, and the impact of lithospheric temperature variations on seismic velocities. This approach aims to further elucidate surface heat distribution, reconcile recent magmatic activity with the substantial elastic thickness observed at Mars' north pole, and explore the compatibility of a thermally driven dynamo with the lifetime of Mars' magnetic field [53].

Currently, it is established that Mars lacks an intrinsic magnetic field. Nevertheless, analyses utilizing data from the Mars Global Surveyor spacecraft have revealed traces of a residual magnetic field on the planet [1, 2]. As highlighted in Ref.[1], the identification of magnetic lineations on Mars suggests that the planet underwent plate tectonic activity in its early history, during which the crust formed through processes akin to sea-floor spreading in the presence of a reversing dynamo, ultimately giving rise to an internal magnetic field. Furthermore, the pioneering work of Langlais, Purucker and Mandea [2] resulted in the development of the first comprehensive model of the Martian magnetic field capable of explaining observations based on potential magnetization distributions. This model served as a valuable tool for predicting the magnetic field and investigating the magnetic characteristics of Mars' lithosphere. Although the exact duration of the lifetime of an internal magnetic field is not known, there is a general consensus regarding the period in time when the dynamo activity may have terminated leading to the termination of the magnetic field. Through studying geologic evidence from the crust of Mars and many simulations, Mars lost its magnetic field 3.6 to 4.1 Gigayears (Gyrs) ago [54, 55, 56]. This range implies a longer lifetime of the dynamo than some previous work which suggested that the cessation of this magnetization of the crust was around 4.115 - 4.13 Gyrs ago [57, 58]. The research conducted by Samuel et al. [3] explores the role of an internally generated magnetic field during the early stages of Mars' evolution as a fundamental factor in comprehension of the thermal history of the planet and its rheological properties. The generally accepted theory posits that the source of Mars' magnetic field is a geodynamo operating within the planet's core. Sustaining this magnetic field necessitates that the thermal energy flow emanating from the core remains above a crucial threshold, ensuring efficient convection of electrically conductive material [4]. In a related study focused on developing a thermal evolution model for Earth, wherein the core remains in a liquid state [5], it was hypothesized that effective mantle temperature reduction is essential to maintain the core-mantle boundary at a temperature conducive to sustained convection. However, the explanation posited in this context for the origin and persistence of Mars' magnetic field was deemed ad-hoc by the authors of Ref.[59]. They proposed an alternative hypothesis suggesting that the Martian core initially possessed a higher temperature compared to the mantle following core formation, resulting in a substantial initial heat flux from the core. Additionally, experimental findings indicated that potassium likely migrated into the Martian core, potentially serving as an additional energy source to sustain a dynamo mechanism.

3.2. Mechanisms that may have ceased the operation of the Martian geodynamo

Various causes have been suggested in the evolution models of Mars for the termination of the dynamo in the core and consequently the magnetic field. The two which will be briefly discussed here are tectonic plates and crater impacts.

Studies have proposed the existence of a periodically reversing magnetic field during the early stages of Mars' development, indicating potential tectonic activity on the planet [4]. In the discussion on the impact of plate tectonics on Mars' magnetic field and thermal evolution, [4] highlights that simplistic models of rocky planet interiors assume convective heat flux to be directly proportional to the mean mantle temperature. Moreover, these models predict a gradual decline in heat flow resulting from the immediate heat production of radioactive elements, assuming a constant and straightforward convective circulation pattern throughout the mantle. However, this cooling process can influence the presence and strength of core convection and dynamo-driven magnetic fields. Due to its its simplicity, this model overlooks several factors, as mentioned in [4]. For instance, it fails to explicitly consider melting, which might have been significant during early Martian history. The paper suggests that plate tectonics or other processes resulting in a large surface heat flux likely induced core convection and magnetic field generation. Conversely, a reduction in surface heat flux might have halted core convection, leading to the cessation of the magnetic field. Thus, the end of Mars' plate tectonic activity could be closely associated with the cessation of its dynamo and magnetic field, potentially resulting in a temporary rise in core temperature. Although an increase in core temperature would lead to more vigorous convective currents and thus a stronger magnetic field, a temporary increase might also create thermal instabilities within the core. These instabilities can disrupt the normal convective patterns by causing localized areas of buoyancy, altering the flow of molten material, and potentially leading to the formation of stagnant regions or differentially heated zones within the core [60]. These effects can disrupt the regular, organized flow of molten material in the interior and may hinder the efficient generation of the planetary magnetic field by impacting the dynamo mechanism. If these disruptions persist or if the thermal perturbation leads to a long-term change in core properties (such as increased viscosity or changes in composition), it could weaken the geodynamo. A weakened geodynamo might ultimately lead to the termination or significant reduction of the planetary magnetic field over an extended period. In essence, this study focused on two possible ways in which the geodynamo could have weakened and lead to the termination of Mars' magnetic field: the end of the plate tectonic regime and/or the decline in surface heat flux throughout geologic time, which is influenced by the half-lives of radioactive isotopes. Additionally, it is demonstrated that models incorporating an early phase of plate tectonics indicate the formation of convective plumes at the core-mantle boundary during the initial 1-2 billion years, followed by a cessation of such activity for several billion years thereafter. Conversely, models devoid of plate tectonics should exhibit consistent plume activity throughout the entire geological record.

Another way in which plate tectonics were studied in regards to the termination of Mars' magnetic field is through considering the transition from an early period of plate tectonics to single-plate tectonics [6]. Early plate tectonics refers to a period in Mars' history when there was active movement and interaction of multiple tectonic plates on the planet's surface. This phase is believed to have occurred during the Noachian and Hesperian epochs [61, 62]. It is mentioned that this phase was also associated with the formation and growth of the Martian crust. Single plate tectonics, on the other hand, refers to a later phase in Mars' evolution when there was a transition from multiple tectonic plates to a single stagnant lid. During this phase, the movement of tectonic plates ceased, and the mantle convection became stagnant. The stagnant lid regime is a convective regime where the outermost regions of the planet's interior are not participating in the flow due to their high viscosity compared to the deep interior. In this regime, conduction dominates in the outer shell, which can be divided into two parts. The deeper section consists of material with a maximum viscosity of about 3 times the mantle viscosity, while the shallower portion is the stagnant lid where convection is absent [4]. The researchers in Ref.[6], Breuer and Spohn, encountered challenges in identifying widely accepted early plate tectonic models capable of adequately explaining both crust formation and the generation of an early magnetic field. Consequently, they suggested that a straightforward thermal evolution model, characterized by gradual cooling of the planet due to stagnant lid mantle convection beneath a single plate, offers a more coherent explanation for early crust formation and magnetic field generation. Hence, the study put forward that the cessation of plate tectonics and the shift to a single plate regime ultimately resulted in the cessation of the magnetic field on Mars.

Through the study of the topography of Mars, focusing on the 20 largest giant impact basins [63], it was found that 15 of them occurred within a 100 Myr period. This corresponds to the early to mid-Noachian period which corresponds to when it is believed that the global magnetic field for Mars disappeared [58]. In Ref.[7], a causal link between this heavy bombardment and the termination of the magnetic field is investigated. This entailed the utilization of three-dimensional spherical mantle convection models along with models incorporating fluctuations in convective intensity and radioactive heating rate. Additionally, control scenarios were conducted for each parameter set, excluding impact heating, enabling the researchers to scrutinize the distinct influence of impact heating on thermal evolution. The models integrated impact-induced heating and accounted for mantle convection to explore the spatial and temporal fluctuations of heat flux at the core-mantle boundary. In order to explore the different possibilities and understand the behaviour of the Martian dynamo under various conditions, both a subcritical dynamo and a supercritical dynamo were considered. A subcritical dynamo refers to a dynamo that operates below a critical heat flow threshold, where a decrease in heat flow can shut down the global magnetic field. On the other hand, a supercritical dynamo operates above the critical heat flow threshold, where an increase in heat flow is required to sustain the magnetic field. It is concluded here that the termination of the dynamo activity in the core of Mars is likely linked to the occurrence of giant impacts, that caused a significant decrease in global heat flow at the core-mantle boundary, leading to a reduction in core heat flow. This drop in core heat flow is primarily due to the heating of the mantle caused by the impact. This heating affects the efficiency of core cooling and thus the heat flow at the core-mantle boundary. The heat flow at the core-mantle boundary is crucial for sustaining core convection and the maintaining of a magnetic field. If this is disrupted significantly the magnetic field can dissipate rapidly.

Building upon the efforts of the aforementioned study, the investigation in Ref.[8] demonstrates that giant impacts on Mars result in thermal stratification in the liquid core, leading to the destruction of a pre-existing core dynamo within ten thousand years. Thermal stratification refers to the layering of different temperatures within a fluid or material. These impacts generate shock waves that deposit heat in the core and mantle. The fluid subjected to this rise in temperature disperses beneath the core-mantle boundary (cmb), generating thermal Rossby waves and moving towards the cmb. At the upper region of the core, the shock-heated fluid expands under the cmb from the sub-impact location, extending to the equatorial plane. The resulting perturbations in temperature and redistribution of shock-heated material establish a stable thermal layering within the core. This layering constitutes of a highly structured region in the outer core, a less stratified zone in the middle, and predominantly adiabatic temperatures in the deeper regions. Consequently, this leads to the suppression of the magnetic field over a period of thousands of years and the hindrance of convection lasting millions of years [8]. It is suggested that convection progressively initiates in the upper regions of the strongly layered area, gradually extending downward over time until all heat induced by impacts is dissipated. Through numerical simulations, the time frame for eliminating core stratification following a significant impact event on Mars was estimated in this work to range from several tens to over one hundred million years.

3.3. Degassing of the Martian mantle

As an alternative to impact heating, the process of magmatic degassing was put forward as the cause for termination of the martian dynamo [9]. The paper proposed the idea that the rapid alterations in mantle convection dynamics stemmed from magmatic degassing during the initial phases of Mars' thermal evolution. This process would cause the mantle to stiffen, resulting in a reduction in the intensity of mantle convection. Due to this, there would be a reduction in core heat flux and therefore weakening and subsequent termination of the dynamo. They conducted numerical simulations employing a model that integrates mantle convection with volatile cycling, incorporating viscosity variations based on temperature and water content. It is noted that the process of making magma in the mantle is influenced by both temperature (through the mantle solidus) and water concentration. Changes in one affect the other, and together they control how much magma is produced. This process creates a partially melted zone in the mantle, and the size of this zone changes as the amount of water in the mantle changes over time. The unique features of their model revolve around the relationships between mantle degassing, mantle rheology, and magmatism. They contemplated Mars as having a stagnant lid atop a convective mantle, which could potentially hinder the efficiency of volatile transfer processes. In this model, mantle degassing is evaluated by measuring the flow rate, denoted by r, of water migrating from the mantle to the crust:

$$r = 4\pi\, R_p^2\, A_{\text{melt}}\, \rho_m\, F_{\text{melt}}\, X_{\text{melt}}\, u_c\, L \tag{6}$$

In the context of this study, several key variables are considered: R_p represents the planetary radius, ρ_m stands for mantle density, and A_{melt} represents the proportion of the mantle undergoing decompression melting, indicating the extent to which melting occurs within the mantle. Additionally, two critical parameters within the mantle melt zone were examined: F_{melt}, which signifies the overall proportion of molten material within this zone, and X_{melt}, indicating the concentration of volatiles within the molten fraction. These parameters, along with u_c representing the velocity of convection, and L as a controlling factor determining the portion of water that is released to the crust, contribute to the understanding of mantle degassing processes. In order to simplify the analysis, both A_{melt} and L were combined into one parameter, termed degassing efficiency factor, denoted by $X_d = A_{\text{melt}}L$. This amalgamation is necessitated by the lack of precise numerical values for both A_{melt} and L. The values attributed to X_d range between 0 and 1, with higher values indicating a greater quantity of water being released from the mantle. In the models outlined in this study, it was assumed that half of the overall heating from radioactivity takes place within the crust. Additionally, they explored scenarios where radioactivity is delivered from the mantle to the crust via magmatic processes. The computational simulations in this work revealed that variations in the degassing coefficient influence both the intensity of the heat transfer rate and the duration of the convective core within a specified parameter range. The findings suggest that a smaller degassing efficiency leads to a longer lifespan of the geodynamo and a higher maximum heat flux. Analysis of the results indicated that higher initial water levels and elevated mantle temperatures contribute to enhanced convective effectiveness, leading to increased heat transfer from the core. Additionally, it was demonstrated that, given reasonable assumptions about degassing efficiency, initial mantle conditions, and water presence, conditions conducive to the establishment of a core geodynamo would persist during the early phases of Mars' evolution. According to the results, the cessation of geodynamo activity on Mars is estimated to occur between 500 and 800 million years following its formation, aligning well with observational data.

This alternative hypothesis for the mechanism behind the cessation of Mars' geodynamo is what underlies all of our work and calculations in this research.

3.4. Effects of dark matter on Earth

There have been several studies on the the interplay between Earth and dark matter. It is imperative to understand this work in order to have a foundation upon which the study of Mars' interaction with dark matter can be built. This is because Earth and Mars are quite similar, with the exception of an ozone layer and magnetic field.

In order to strengthen the volcanic hypothesis' viability, Abbas and Abbas [12] introduced Volcanogenic dark matter. The volcanic hypothesis states that periodic volcanic activity on Earth is the primary reason for mass extinctions of various species throughout geological history. This notion finds support in the alignment between the ages of numerous significant flood basalt provinces and the timing of major paleontological mass extinctions [64]. The creation of these massive basalt provinces is attributed to intervals of large-scale basalt volcanism which is preceded by explosive silicic volcanism. This form of volcanism is caused by the arrival of a rising plume, which is created by the lowermost layer of the mantle continuously absorbing heat, to the surface of the crust resulting in the production of viscous acidic magma [64, 65]. Ref.[12] suggests that the traversal of Earth through concentrated clusters of dark matter is what leads to the excess heat produced in the interior of Earth, through gravitational capture and resulting annihilation. Thus, they put dark matter forward as the leading cause behind this violent volcanism and these mass extinctions.

In 2014, Rampino [13] expanded on this while investigating the relation between the periodicity of geological events and galactic dynamics. It was suggested that the Sun's vertical oscillations through the galactic plane influence our solar system's interaction with visible matter concentrated in the galactic mid-plane, as well as its interaction with disk dark matter. This study explored the estimates for the time between plane crossings and compared them to the estimates found for the dates of major impacts and mass extinctions. Given the proposal that the Oort comet cloud might experience gravitational disturbances due to the passage through the Galactic plane, caused by Galactic tidal forces originating from visible matter [66, 67, 68], this research extends the examination to include disk dark matter as an additional source of galactic tidal forces. These perturbations could potentially result in recurring meteor showers in the inner Solar System, leading to terrestrial impacts and corresponding mass extinctions on Earth. Moreover, the investigation explores the periodic interaction of Earth with dense clusters of dark matter as one potential rationale for the episodic occurrences of terrestrial phenomena such as volcanism, geomagnetism, and plate tectonics. This exploration aimed to provide insight on how the capture of dark matter particles could contribute to mass extinction events.

The reason that the Earth still has a magnetic field, despite its interaction with dark matter, is mainly attributed to its tectonic activity, something which Mars does not possess at all. The Earth's magnetic field is maintained by its geodynamo, which is driven by the movement of molten iron in the planet's outer core. This movement is influenced by several key mechanisms. Tectonic activity plays a crucial role in the recycling of the Earth's crust, which contributes to the heat flow and convection currents within the mantle and core. These currents facilitate the continuous motion of molten iron. Additionally, the ongoing recycling and movement of the Earth's crust help sustain the temperature differences needed to drive these convection currents. Due to these ongoing processes, the activity of the geodynamo continues, thus maintaining its magnetic field.

Due to the similarities between Earth and Mars, we may extend many of the hypotheses formed for Earth in relation to dark matter, to Mars.

4. Method,Analyses and Results

4.1. Earth's interaction with dark matter clumps

In the following work, it is assumed that dark matter is entirely made of WIMPs. The first step in our work was to replicate the values, for the heat produced in the Earth due to dark matter capture and annihilation, previously obtained in Refs. [12] and [13]. The formula they used to calculate the heat generation is:

$$Q_e = \mathrm{e}\,\mathrm{N_e}\,\mathrm{m}_\chi \tag{7}$$

where e denotes the proportion of annihilations contributing to the generation of heat in the interior of Earth (set to ~ 0.5 in their calculations), m_χ represents the mass of the WIMP, and N_e is the capture rate of WIMPs as devised by [69]:

$$N_e = (4.7 \times 10^{17}\,\mathrm{s}^{-1})(3ab)(\rho_{0.3}\,v_{300}^{-3}\,\sigma_{N,32})(1 + m_\chi^2/m_N^2)^{-1} \tag{8}$$

where $\mathrm{m_N}$ is the mass of the ordinary matter nucleus, which interacts with a WIMP through elastic scattering with a cross-section denoted as σ_N. Additionally, ρ_χ is the local average density of WIMPs, while v represents the local rms velocity of the dark matter particles. Furthermore,$\sigma_{N,32}$ is the interaction cross-section normalized to $\sigma_N/10^{-32}\mathrm{cm}^2$, $\rho_{0.3}$ is the WIMP density normalized to 0.3 $\mathrm{GeV\,cm^{-3}}$, and v_{300} is the velocity normalized to 300 $\mathrm{km\,s^{-1}}$. The coefficients a and b are determined by the Earth's density profile. Abbas & Abbas [12] employed specific values for these parameters: $\rho_{0.3} = 1$, $ab = 0.34$, $v_{300} = 1$, the iron cross-section $\sigma_N = 10^{-32}\,\mathrm{cm}^2$, and WIMP masses ranging from 15 to 100 GeV. They considered iron to make up the entire core of the Earth and found that heat generated from the movement of Earth through a dense clump of dark matter could be as high as 10^{16} watts. In the case of uniform dark matter density, the heat generated was found to be at most 10^8 watts.

To validate the formulae from a recently published paper by Leane and Smirnov [14] (which we intended to use for our calculations), we employed the provided functions for iron only, using the same WIMP-mass range as above, to calculate and compare heat injection. We calculated the heat power produced by dark matter (Γ) as follows:

$$\Gamma = m_\chi f C_{\max} \tag{9}$$

where m_χ is the mass of the WIMP, f is the fraction of captured DM particles, and $C_{\max}$ is the maximal capture rate given in Ref.[70]:

$$C_{\max} = \pi R^2 n_\chi(r) v_0 \left(1 + \frac{3}{2}\frac{v_{\mathrm{esc}}^2}{v_d^2}\right) \tag{10}$$

Here, R is the planetary radius ($\sim$ 6371 km for Earth [71]), $n_\chi(r)$ indicates the density of the dark matter particles at a distance r from the galactic centre, v_0 represents the average speed in the dark matter rest frame, which is associated with the velocity dispersion v_d at a distance r from the galactic centre. The escape velocity of the planet is denoted by v_{esc}, which is ~ 11.18 km/s for Earth. By using the fact that $\rho_\chi = n_\chi m_\chi$, the heat power then takes the form:

$$\Gamma = f\pi R^2 \rho_\chi(r)\, v_0 \left(1 + \frac{3}{2}\frac{v_{\text{esc}}^2}{v_d^2}\right) \tag{11}$$

The fraction of WIMPs that are passing through the planet and being gravitationally captured as defined in Ref.[14] is:

$$f = \frac{C_{\text{cap}}}{C_{\text{max}}} = \sum_{N=1}^{N_{s,\text{max}}} f_N \tag{12}$$

where f_{N_s} is the capture fraction for a specific number of scatterings of the dark matter particle. This is given as:

$$f_{N_s} = p(N_s, \tau)\left[1 - \kappa \exp\left(-\frac{3(v_N^2 - v_{\text{esc}}^2)}{2v_d^2}\right)\right] \tag{13}$$

where p(N,τ) is the probability that a WIMP scatters N_s times. This was formulated by Ilie, Pilawa and Zhang [72] as:

$$p(N_s, \tau) = \frac{2}{\tau^2}\left(N_s - \frac{\Gamma(N_s + 2, \tau)}{N_s!} + 1\right) \tag{14}$$

where τ is the optical depth and Γ (a,b) is the incomplete gamma function , $\tau = \frac{3}{2}\sigma/\sigma_{\text{sat}}$ where σ is the dark matter-target interaction cross-section, and σ_{sat} which is saturation cross-section $= \pi R^2/\text{N}_{\text{SM}}$. N_{SM} is the number of target particles. κ is defined as:

$$\kappa = \frac{1 + \frac{3}{2}\frac{v_N^2}{v_d^2}}{1 + \frac{3}{2}\frac{v_{\text{esc}}^2}{v_d^2}} \tag{15}$$

where $v_N = v_{\text{esc}}\left(1 - \langle z\rangle \frac{4m_\chi m_A}{(m_\chi + m_A)^2}\right)^{-N_s/2}$. The average scattering angle, $\langle z\rangle$, is taken to be 1/2 by [72], and m_A represents the mass of the target particle.

Taking the mass of an iron nucleus and the same value for the interaction cross-section as that in Ref.[12], when ranging the WIMP mass from 15 to 100 GeV, we found that the highest possible value for heat production from dark matter annihilation, as seen in Figure 6 was $\sim 10^9$ Watts, if Iron was assumed to make up the entire core of Earth. The values seen in the work [14] ranged from 10^5 to 10^9 Watts, meaning that we had successfully replicated their results.

Now that it was confirmed that the formulae from Ref.[14] are sensible, we extended the calculation to account for all of the main elements that Earth's core consists. The elements considered are iron, silicon, sulphur, magnesium, oxygen, nickel, aluminium, and calcium. The proportion of these elements in the Earth's mass was accounted for in the calculation for N_{SM}.

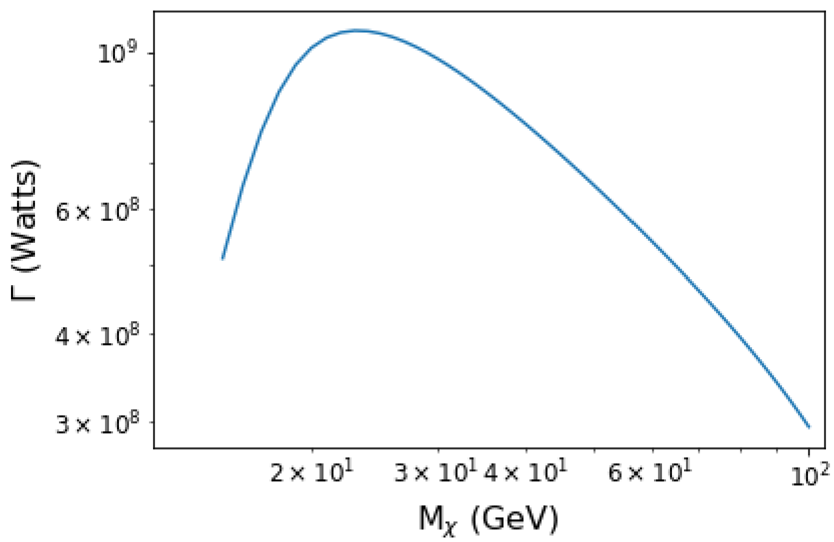

Figure 6 : Heat flow graph obtained from the formalism provided by [14], keeping the interaction cross-section for Iron = 10^{-42} km^2, assuming that it to fully constitute the Earth's core.

While deriving the rigorous formula for the capture rate of WIMPs by a massive body, Gould [11] noted that there are resonant enhancements in the capture when the mass of the WIMP is similar to that of the nucleus of the target element, leading to a much larger overall capture rate than previously believed. The interaction cross-section used in this derivation was devised by [73] as:

$$\sigma = \frac{\mu}{\mu_+^2}(N - 0.124Z)^2\frac{m_\chi m_A}{\text{GeV}^2} \times 5.2 \times 10^{-40}\text{cm}^2 \qquad (16)$$

with $\mu = \frac{m_\chi}{m_A}$, $\mu_+ = \frac{\mu+1}{2}$, Z being the number of protons and N the number of neutrons in the nucleus of the target atom. This implies that the interaction cross-section is is contingent upon both the element in consideration, as well as the mass of the dark matter particle. Since both [12] and [13] used this formulation for the cross-section, we inserted this for σ in our heat power calculations. Once the heat power output was calculated from the scatter with each element and subsequent annihilation, the heat power values were summed up to output a single heat value corresponding to a specific WIMP mass. We considered both scenarios of a single scattering, as well as a large number of scatterings for the WIMP. As can be seen in our plot in Figure 7, the maximum heat flow obtained here is $\sim 10^{15}$ Watts, which quite close to the maximum value obtained by [12] when considering interaction with a dense dark matter clump. However, the maximum heat flow value obtained by us for 1 scattering is $\sim 10^{10}$ Watts, which is extremely close to the maximum heat flow for a uniform dark matter density obtained in Refs. [13] and [11]. The difference can be accounted for by the fact that we did not assume Iron to make up the entire core of the planet, and we additionally considered multiple scatterings. The comparison above shows the significant effect of a large number of scatterings; even while assuming a uniform dark matter density, the value of maximum heat flow obtained from considering a large number of scatterings is the same as the heat flow obtained for a single scattering when regarding interaction with a clump of dark matter.

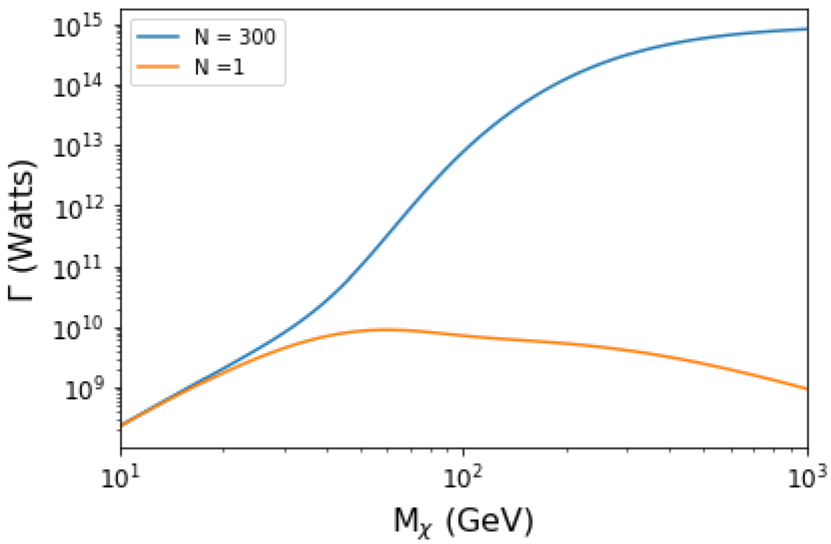

Figure 7 : Heat Flow graph obtained from the formalism provided by [14], by varying the interaction cross-section for each element-WIMP mass pair. The WIMP mass range is kept as 15 - 100 GeV. A single scattering and multiple scatterings are considered here. The WIMPs would scatter off the ordinary matter atoms, be gravitationally captured on Earth and subsequently annihilate.

The formulation of the cross-section in Equation 16 only tells us how likely a collision will be based on the masses of the two particles involved. However, as can be seen from Figure 7, the resonance effect predicted in the work [11] is not yet seen. The capture rate for each element, including resonant enhancement, as derived by Gould is as follows:

$$C = 4 \times 10^{16}\,\mathrm{s}^{-1} \rho_{0.4} \frac{\mu}{\mu_+^2} Q^2 f \left\langle \phi \left(1 - \frac{1 - e^{-A^2}}{A^2} \right) \xi_1(A) \right\rangle \tag{17}$$

where f is the proportion of the Earth's mass due to this element, $\rho_{0.4}$ is the WIMP density of the halo normalized to $0.4\,\mathrm{GeV\,cm^{-3}}$, $Q \approx N - 0.124Z$, $\xi_1(A)$ is a correction factor where $A^2 = \frac{3v^2\mu}{2v_\mathrm{d}^2\mu_-}$, v is the maximum velocity of the WIMP post-scattering, v_d is the velocity dispersion, $\mu_- = \frac{\mu-1}{2}$, and $\phi = \frac{v^2}{v_\mathrm{esc}^2}$ is the dimensionless gravitational potential. The capture rates calculated by [11] using this were significantly higher than previously believed. For an isotropic dark matter density, the heat production found here was $\sim 10^8 - 10^{10}$ Watts, whereas for a dense clump of dark matter, the heat flow was found to be $\sim 10^{16} - 10^{18}$ Watts.

We modified the formalism seen in Equations 9 to 15 from Ref.[14] in order to account for this resonant enhancement. We introduced a resonance factor of $\frac{\mu}{\mu_-^2}$. The equations for f_N and κ then become:

$$\kappa = \frac{1 + \frac{3}{2}\frac{\mu}{\mu_-^2}\frac{v_N^2}{v_d^2}}{1 + \frac{3}{2}\frac{\mu}{\mu_-^2}\frac{v_\mathrm{esc}^2}{v_d^2}} \tag{18}$$

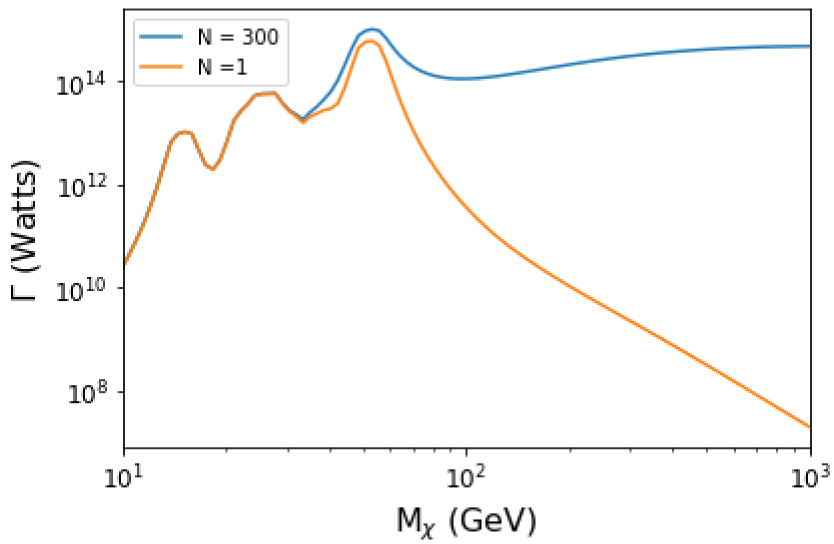

Figure 8 : A graph showing the total heat power output from the interaction of WIMPs with all of the elements in the core of the Earth, accounting for the resonant enhancement. This uses Gould's formulation for the interaction cross-section.

$$f_{N_s} = p(N_s, \tau)\left[1 - \kappa \exp\left(-\frac{\mu}{\mu_-^2}\frac{3(v_N^2 - v_{\text{esc}}^2)}{2v_d^2}\right)\right] \tag{19}$$

The resulting plot can be found in Figure 8. It is seen here that our prediction was indeed correct; there are resonant peaks occurring where the the target particle mass equals the mass of the WIMP, in units of GeV. This is logical from the laws of kinematics: maximum energy and momentum transfer will occur when two objects of the same mass collide head on. The peaks represent this maximum transfer for each element. The two largest peaks are due to iron and oxygen, respectively. This is due to the fact that these are the two most abundant elements in the Earth. Additionally, the effect of the number of scatterings on the heat power, should be noted. It can be seen that at large WIMP masses, a large number of scatterings will yield a much higher heat power value, as opposed to a single scattering which yields a decline in the heat power. The heat power eventually stabilises when a large number of scatterings is considered. This is likely attributable to the fact that when a dark matter particle is scattered multiple times, it becomes much easier for it to be gravitationally captured as it loses energy with every collision. The difference between N = 1 and N = 300 is larger when resonance is included, which suggests multiple scatterings need to be considered due to the mass mismatch between heavy WIMPs and the target nuclei reducing energy transfer during collisions. The two effects: resonance and multiple scatterings are not independent in their effect on the capture rate and need to be considered together.

To compare the cross-sections we obtained to those provided by recent observations, we used the 2018 data from the Xenon1Ton experiment [74]. Utilizing the plot depicting the interaction cross-section between WIMPs and nucleons as a function of WIMP mass, we employed interpolation

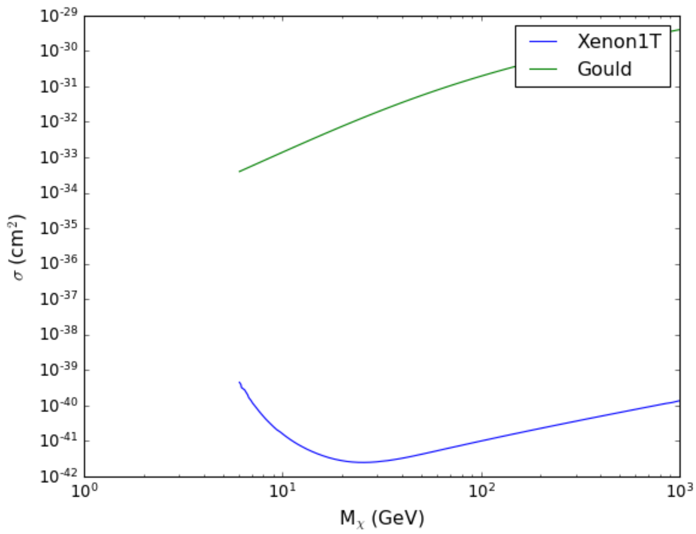

Figure 9 : A comparison between Gould and Xenon1Ton of the atomic cross-sections as a function of WIMP-masses, for the element of iron.

techniques to derive a functional relationship representing the WIMP-nucleon cross-sections across varying WIMP masses. This was then converted to give the WIMP-nucleus cross-sections as a function of WIMP mass. This was obtained as follows:

$$\sigma_{\text{nucleus}} = \sigma_{\text{nucleon}} \times (N+Z)^2 \times \frac{\frac{m_\chi m_A}{m_\chi + m_A}}{\frac{m_\chi(1)}{m_\chi+1}} \tag{20}$$

By limiting our WIMP-mass range, to that explored only by Ref.[74], we can compare the atomic interaction cross-sections from Gould to those from Xenon. This was first done for iron only and can be seen in Figure 9. It can be seen in this figure that the cross-sections from Gould are significantly larger than those from Xenon. A possible explanation for this is that Gould's is a conjectured extrapolation from quite some time ago, whereas Xenon are the latest empirical limits. It can be seen that the estimates produced by [12] and [13] are weak when they use Gould's formulation for the cross-sections.

Since the limits from Xenon are more stringent, we proceeded with the interpolated function to plot the atomic cross-sections for all of the elements in the core, over the same WIMP-mass range (Figure 10).

These cross-sections were then fed into our calculation for the heat power produced to give a new plot of heat ouput vs WIMP-mass, as seen in Figure 11. The values for m_χ considered are 15 - 100 GeV and the number of scatterings N is set to 100. The plot includes both the results with and without the inclusion of the resonance factor for comparison. The resonance effect is still prominent here, but the heat power values have dropped by quite a few orders of magnitude. The peak corresponding to Iron is around 10^9 now, whereas it was $\sim 10^{15}$ in Figure 8. A similar drop can be seen in the resonant peak for Oxygen. This is owing to the fact that the interaction cross-sections from Xenon are much smaller as compared to those from Gould.

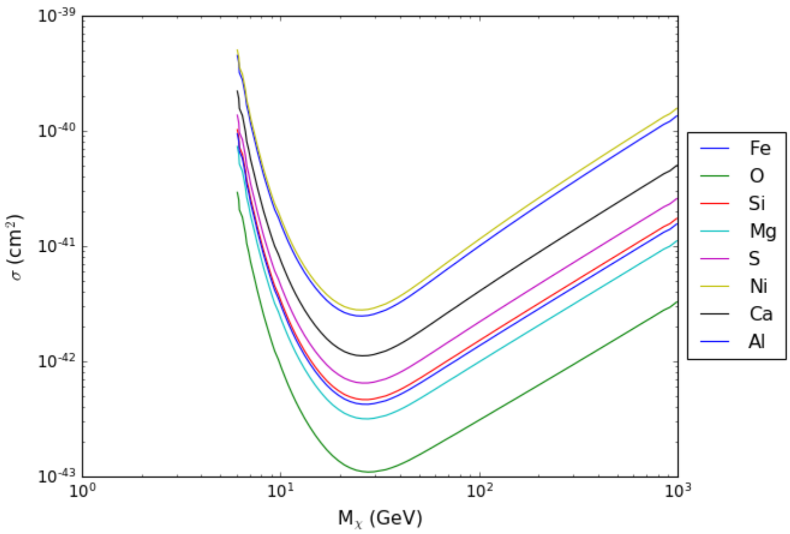

Figure 10 : Plot of nucleus-WIMP interaction cross-sections as a function of the masses of WIMPs, for all eight elements in the core.

It should be noted here that we would need a much larger dark matter density to get better results since it is the only parameter that could potentially change to boost heat flow. The volcanogenic hypothesis is unviable with only the smooth local DM density of the Milky-Way, hence we consider clumps.

Taking into account the fact that the Earth has a heat output of $\sim$ 44 TW [75], we used the aforementioned data to calculate limits on the cross-sections for all the elements. The assumption we used here is that all of the heat produced from Earth was due to dark matter annihilation, which is a highly conservative scenario, in that it will produce the weakest possible limits on dark matter. In Figure 12, the shaded area represents interaction cross-section values which have been excluded at a 95 % confidence level. This means that the excluded cross-sections are too large and would produce more heat flow than is currently observed. When comparing the values we obtained to the ones found by Bramante et al. [75], our calculations have excluded cross-sections that are smaller by several orders of magnitude. It should be noted that when trying to expand our mass-space to cover the same masses as those in Ref.[75], we found that outside of the range presented in Figure 12, the heat flow rate never becomes significant. The large number of needed collisions for the heavy mass mismatch results in a strong suppression of scattering probability in Equation 14. This is a major difference to [75] whose formalism allows all masses to produce significant heating. This could again be attributed to the fact that resonances were not accounted for in this work. Furthermore, upon testing various large numbers of scatterings, we found no significant difference between the case of N = 100 and N = 200 or N = 300.

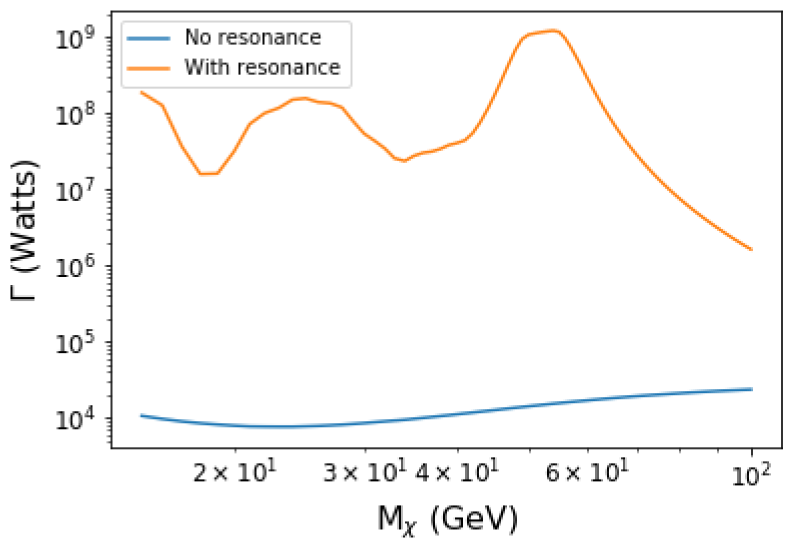

Figure 11 : Heat produced as a function of WIMP-mass, using the cross-sections obtained from Xenon1Ton [74] data. The number of scatterings considered is 100.

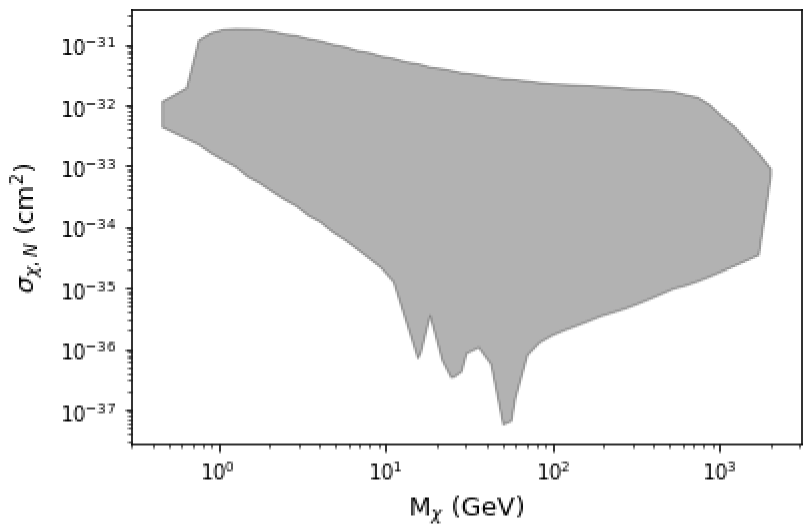

Figure 12 : Cross-sections that are excluded at a 95% confidence level are shown by the shaded region. The number of scatterings used here is N = 100.

4.2. Heat injection on Mars from dark matter annihilation

All the calculations were then performed again, with the changes being that the radius ($\sim$ 3389.5 km [71]) and escape velocity ($\sim$ 5.01 km/s) of Mars were used instead of Earth's. The plot of heat power vs m_χ, using Gould's formulation of the atomic cross-section can be seen in Figure 13, and the same plot using Xenon's data for the atomic cross-section can be found in Figure 14. Comparing to the plots we acquired for Earth, it can be seen that the overall heat power values are slightly lower for Mars. It can also be seen that there is a larger number of well-defined peaks in the case of Mars. Similar to the case for Earth, the Xenon limits once again provide lower heat values than Gould.

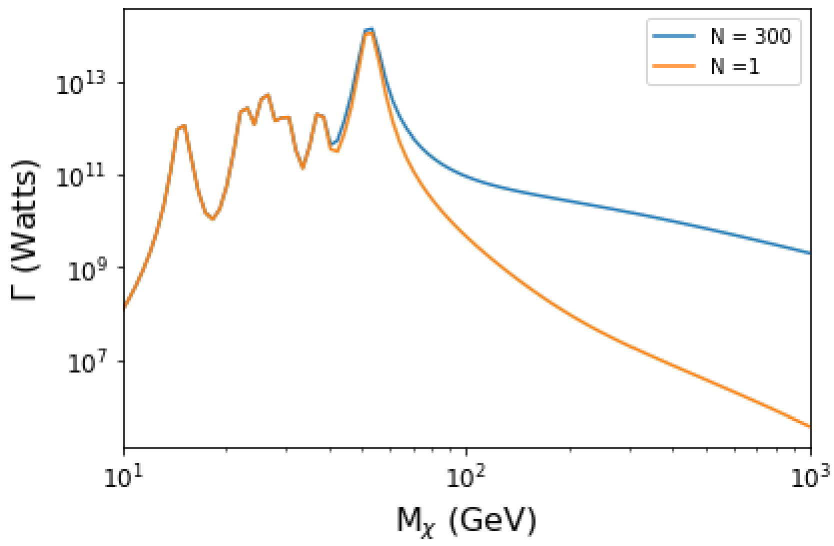

Figure 13 : Heat produced, Γ , as a function of WIMP-mass, using Gould's formulation of the atomic cross-section, accounting for resonance.

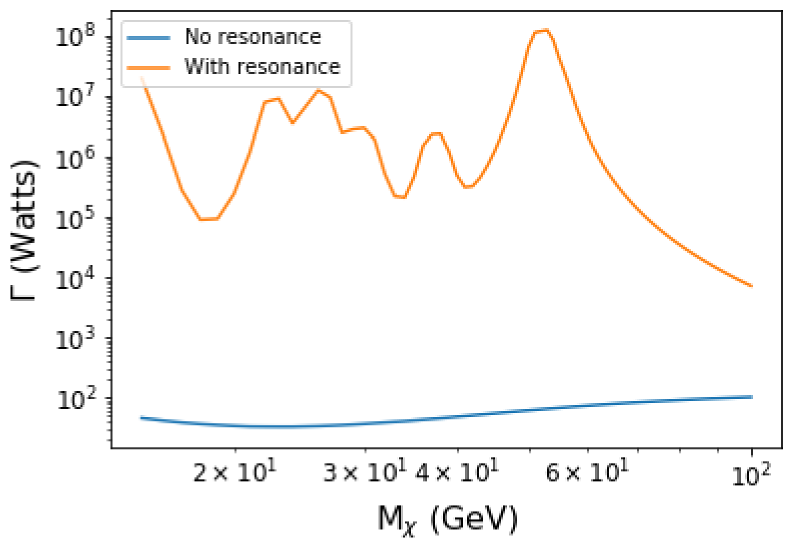

Figure 14 : Heat produced, Γ , as a function of WIMP-mass, using the atomic cross-sections calculated using Xenon's interpolated function. The number of scatterings was set to 100.

Using the results from the work of Parro et al. [76], which found the heat flow on Mars to range from 14 to 25 $\mathrm{mWm^{-2}}$, the prospective heating exclusion limits for Mars due to s-wave dark matter self-annihilation, were deduced by [75]. This was compared to the the exclusion limits we calculated for the DM-nucleon cross-section (see Figure 16). The cross-sections excluded by [75] range from 10^{-36} to $10^{-13}\mathrm{cm}^2$, whereas the ones found in this work range from 10^{-38} to $10^{-30}\mathrm{cm}^2$. The WIMP masses we considered had a narrower range than than those considered by the previous work. It should be noted that when trying to expand our WIMP mass range and excluded cross-sections to match those of [75], it was observed that regardless of how arbitrarily large the chosen WIMP-nucleon cross-sections get, WIMPs above ∼ 1900 GeV and below ∼ 0.5 GeV do not produce enough heat flow to be excluded. This shows that our work was able to exclude much smaller cross-sections as compared to previous work. This could be attributed to the fact that the previous work had not considered the effect of resonant enhancements in their calculations.

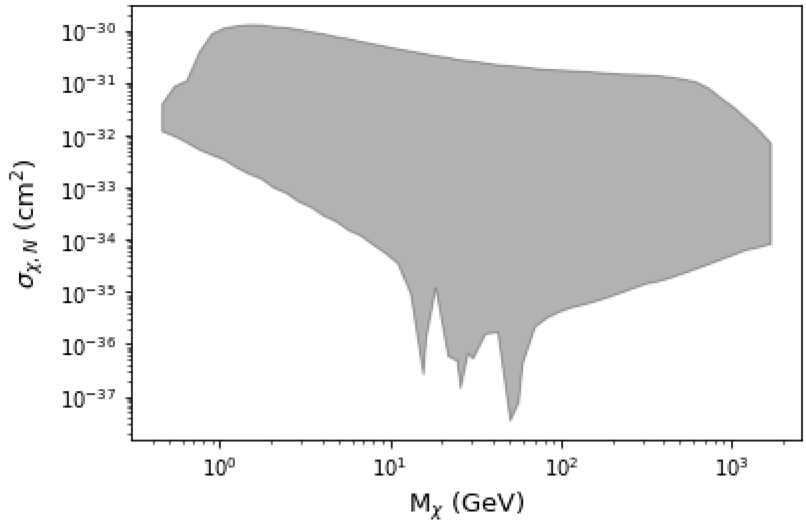

Figure 15 : WIMP-nucleon cross-section exclusion limits for Mars at a 95% confidence level.

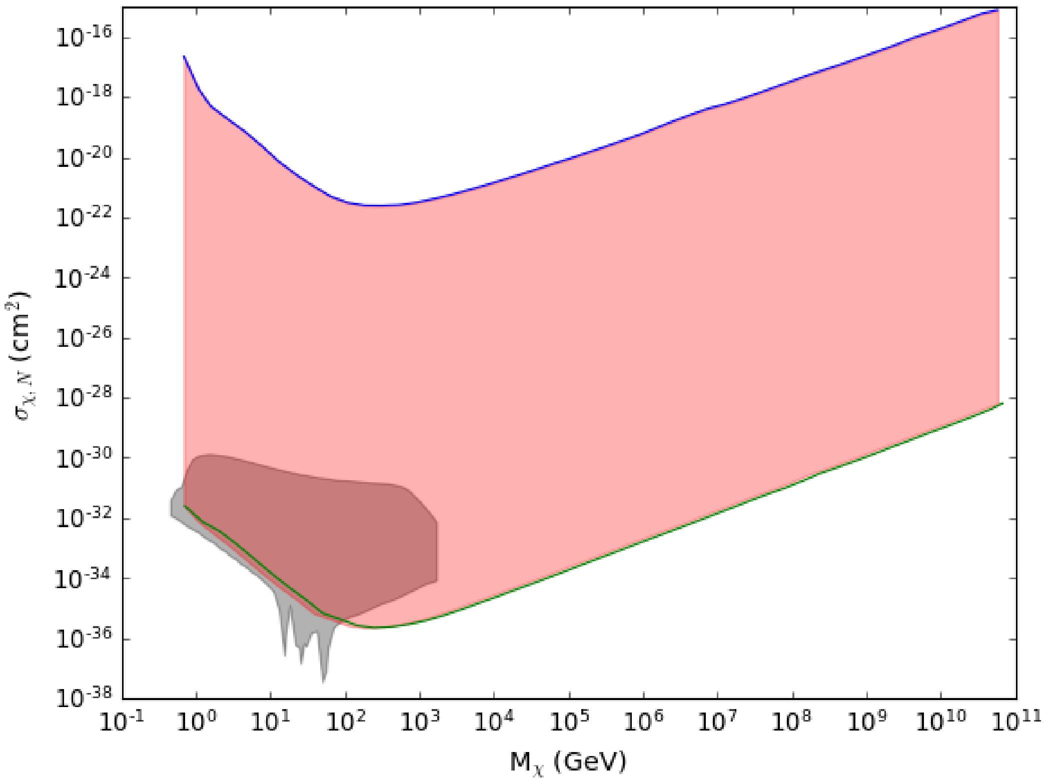

Figure 16 : The exclusion region from [75] (in red) layered over the our exclusion limits (in grey).

It is worth noting that the exclusion limits plot for Mars has much sharper peaks than that of Earth. This could be due to the fact that Mars is an order of magnitude less massive than the Earth and has almost half the radius of Earth. There are two variables that are strongly influenced by the mass and radius of the planet under consideration: σ_{sat} and V_{esc}. The saturation cross-section for Mars is 2.5 times that of Earth's making the optical depth, τ, 2.5 times smaller for Mars than for Earth. Additionally, the escape velocity for Mars is 5 times smaller as compared to the value for Earth, making it more difficult for WIMPs to be captured by Mars. This makes the resonance effect more important for Mars as it is easier to mitigate a smaller escape velocity for WIMPs of resonant masses. The masses above and below the resonant masses are far more difficult to capture and thus produce less heat output than those at the resonance. Due to these pronounced effects in the case of Mars, the peaks are steeper.

4.3. Likelihood of dark matter annihilation terminating dynamo activity in the Martian core

The minimum threshold value for heat flux out of the convective core on Mars is thought to be between 5 and 19 mWm^{-2} [4]. We chose the value of 10 mWm^{-2} for the critical heat flux since that is approximately halfway, and this specific value was shown to result in a minimum lifetime of 500 Myrs for the geodynamo of Mars [9]. This value was then converted into a total heat power output for Mars and used as the threshold value in calculating how dense a dark matter clump would have to be to significantly affect the activity of the core.

The first step was calculating the boost factors as a function of WIMP masses. This would tell us how much greater, for a certain m_χ, the density of a dark matter clump needs to be than the local solar dark matter density. The boost factor is defined as:

$$b = \Gamma_{\text{req}}/\Gamma_{\text{ref}} \,. \tag{21}$$

where Γ_{req} is our critical heat output i.e. $10^{-3} \times 4\pi R_{\text{Mars}}^2$ and Γ_{ref} is an array of all of the total heat output values calculated from the interpolated function obtained using Xenon1Ton's cross-sections data from 2018 [74]. We can then find the required densities as a function of WIMP-mass by:

$$\rho_{\chi,\text{req}} = b \times \rho_{\chi,\odot} \,. \tag{22}$$

where $\rho_{\chi,\odot}$ is the dark matter density in our solar system $\approx 0.42\,\text{GeV/cm}^3$ [77]. The connection between required densities and the dark matter particle masses can be seen in Figure 17.

In order to find the smallest concentration parameter c_{vir} of our required sub-halos, we minimized the following function:

$$3\rho_s \frac{\int_0^{c_{\text{vir}}} \frac{x^2}{x^{1.5}(1+x^{1.5})}}{c_{\text{vir}}^3} dx - \Delta_c \rho_{\text{crit}} = 0 \tag{23}$$

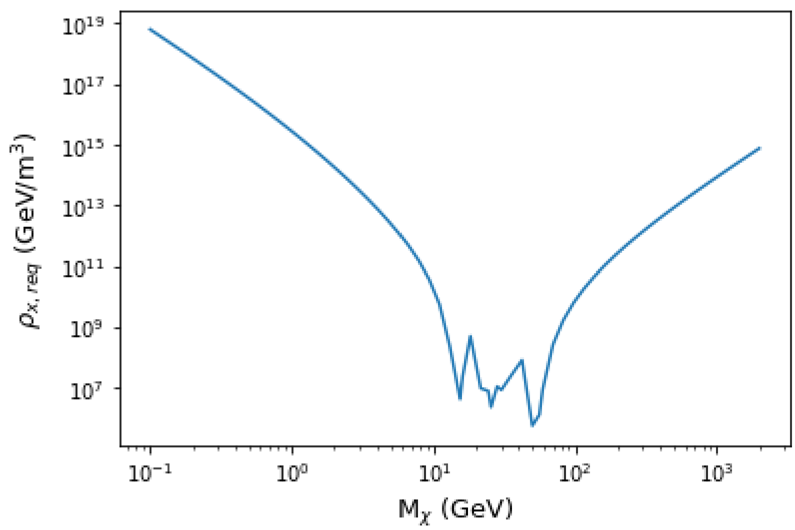

Figure 17 : Required dark matter densities, as a function of WIMP-mass.

where Δ_c is the critical density contrast for collapse. It expresses the overdensity required for a region of the universe to overcome the cosmic expansion and eventually collapse to form a bound structure. For a ΛCDM model of the universe, at the present epoch (z = 0), it is ≈ 100 [78]. The integrand times by ρ_s is the Moore dark matter density profile [40], where $x = \frac{r}{r_s}$. The x^2 in the numerator accounts for the volume element in spherical coordinates, due to the spherical symmetry of the halo. The scale density ρ_s was set to the smallest $\rho_{\chi,\mathrm{req}}$ value i.e. $5.7 \times 10^5 \mathrm{GeV/m^3}$ as ρ_s gives an idea of the density in the central region of the clump. The average clump density was found to be $1.51 \times 10^7 \mathrm{M_\odot/kpc^3}$. This implies that the clump would have to be 4.3 times denser than the Milky Way galaxy.

The result from the minimization and numerical integration gives c_{vir} as 7.93. Using a relationship between $\mathrm{c_{vir}}$ and $\mathrm{M_{vir}}$ deduced by Comerford and Natarajan [79]:

$$c_{\mathrm{vir}} \approx \frac{14.5}{1+z}\left(\frac{M_{\mathrm{vir}}}{1.3 \times 10^{13} h^{-1} M_\odot}\right)^{-0.15} \tag{24}$$

we find that for a redshift of 0 with the c_{vir} value we found, the mass of the sub-halo would have to be $\sim 3.43 \times 10^{11}$ $\mathrm{M_\odot}$. This is around 0.25 of the mass of the Milky Way [80] which makes a sub-halo with a large mass such as this, highly unlikely.

However, an ultra-compact dark matter mini-halo (UMCH) is formed quite differently and could be quite dense, while having the same c_{vir} as found in Ref.[81]. Here, a power spectrum spike model is assumed. Using a scale radius r_s of 10^{-4} Kpc [82] and a concentration parameter = 7.93, we find $\mathrm{m_{vir}}$ as follows:

$$\mathrm{m_{vir}} = 4\pi r_s^3 \rho_s \int_0^{\mathrm{c_{vir}}} \frac{x^2}{x^{1.5}(1+x^{1.5})} dx \tag{25}$$

This resulted in $m_{vir} \sim 3.09 \times 10^{-1} M_{\odot}$. Now using this as our mini-halo mass, we can calculate the number of encounters such a halo would have with Mars over a specified time period:

$$\text{No. of encounters} = v_{\text{sys}}\, \sigma_{r_s}\, \rho_{\chi,\odot}\, \text{time period}\, \frac{f_h}{\text{m}_{\text{vir}}} \tag{26}$$

After specifying the speed of our solar system around the galaxy v_{sys} as 220×10^5 cm/s, the cross-sectional area (with radius $= r_s$) for interaction with a planet σ_{r_s} as 1.2×10^{36} cm^2, the local dark matter density as 3.59×10^{-58} $M_{\odot}/cm^3$, and the proportion of dark matter in the form of mini-halos f_h as 10^{-3} [83], we find that the number of encounters in 1 Gyr is 8.60×10^2. This is a large number of interactions , as we only require the halo to get within r_s of the planet. It is observed that the number of encounters scales with $1/r_s$. This calculation assumes that all UCMHs are the same mass and radius. This probably would not be true and would reduce the number of encounters. However, it can be seen that there is a decent probability that we encounter such an object in 1 Gyr. Further improvement on this result can be done by considering the exact distribution of UCMH halos and the variability in their masses and sizes.

5. Conclusion

In this work, we have successfully replicated results from previous work regarding heat injection in Earth's core from dark matter annihilation, but using a much more recent formulation. We then extended the work to account for resonant enhancements. This was first done by [11] but none of the other works in consideration, including quite recent ones, accounted for that. We modified the recent formulations to include these resonant effects from all of the elements in the Earth's core. Once it was verified that this modified formulation produced sensible results, we then went on to compare what was previously obtained to the latest empirical limits from [74], for the exclusion limits on the WIMP-matter interaction cross-sections. We then proceeded with finding the heat produced, using the more stringent empirical limits, and deducing our own exclusion limits for Earth at a 95% confidence level. These limits were calculated using the maximum heat flow found for the Earth.

This method was then performed for Mars, producing similar results in using both the conjectured extrapolation for the interaction cross-section, as well as the most recent empirical findings. The exclusion limits were also found for Mars at a 95% confidence level. The only values that were changed for this were the mass, radius and the heat flow threshold for Mars. Comparing our results to previous work such as [75], we find that our work excludes even smaller cross-sections due to the consideration of multiple scatterings in addition to the effect of resonance enhancements in the capture rate. Proceeding with our calculated heat injection values for Mars, we found how much more dense dark matter sub-haloes would have to be than the local dark matter density, in order to exceed the threshold for Mars' heat flow. We found that a normal sub-halo would need to be ~ 4 times more dense than the Milky Way and have a mass of around $3.43 \times 10^{11} \mathrm{M}_{\odot}$. A sub-halo such as this is highly unrealistic. Thus, we then considered an ultra-compact mini-halo, which forms differently and is able to achieve an extremely high density. When changing the parameters to those for an UCMH, we find a virial mass of $0.309\ \mathrm{M}_{\odot}$, which is much easier to come across. Using this as our mini-halo mass, we found that the possible encounter rate for such a halo and a planet in our solar system (Mars for the purpose of our work), is ~ 860 per Gyr. This shows that there is a relatively good chance of Mars interacting with a dark matter halo that would lead to the termination of its geodynamo. It should be noted that this is under the assumption that all UCMHs are of the same mass and density, and that the fraction of these halos is 10^{-3} of all dark matter. Consideration of the variation in the masses of these halos, as well as their distribution throughout the universe, may lower the aforementioned probability.

References

[1] J. E. P. Connerney et al. 'Tectonic implications of Mars crustal magnetism'. In: *Proceedings of the National Academy of Sciences* 102.42 (2005), pp. 14970–14975. DOI: `10.1073/pnas.`

0507469102. eprint: https://www.pnas.org/doi/pdf/10.1073/pnas.0507469102. URL: https://www.pnas.org/doi/abs/10.1073/pnas.0507469102.

[2] B. Langlais, M. E. Purucker and M. Mandea. 'Crustal magnetic field of Mars'. In: *Journal of Geophysical Research: Planets* 109.E2 (2004). DOI: https://doi.org/10.1029/2003JE002048. eprint: https://agupubs.onlinelibrary.wiley.com/doi/pdf/10.1029/2003JE002048. URL: https://agupubs.onlinelibrary.wiley.com/doi/abs/10.1029/2003JE002048.

[3] Henri Samuel et al. 'The rheology and thermal history of Mars revealed by the orbital evolution of Phobos'. In: *Nature* 569.7757 (2019), pp. 523–527. DOI: 10.1038/S41586-019-1202-7.

[4] F. Nimmo and D. J. Stevenson. 'Influence of early plate tectonics on the thermal evolution and magnetic field of Mars'. In: *Journal of Geophysical Research: Planets* 105.E5 (2000), pp. 11969–11979. DOI: https://doi.org/10.1029/1999JE001216. eprint: https://agupubs.onlinelibrary.wiley.com/doi/pdf/10.1029/1999JE001216. URL: https://agupubs.onlinelibrary.wiley.com/doi/abs/10.1029/1999JE001216.

[5] G. Schubert, P. Cassen and R.E. Young. 'Core cooling by subsolidus mantle convection'. In: *Physics of the Earth and Planetary Interiors* 20.2 (1979), pp. 194–208. ISSN: 0031-9201. DOI: https://doi.org/10.1016/0031-9201(79)90043-8. URL: https://www.sciencedirect.com/science/article/pii/0031920179900438.

[6] D. Breuer and T. Spohn. 'Early plate tectonics versus single-plate tectonics on Mars: Evidence from magnetic field history and crust evolution'. In: *Journal of Geophysical Research: Planets* 108.E7 (2003). DOI: https://doi.org/10.1029/2002JE001999. eprint: https://agupubs.onlinelibrary.wiley.com/doi/pdf/10.1029/2002JE001999. URL: https://agupubs.onlinelibrary.wiley.com/doi/abs/10.1029/2002JE001999.

[7] J.H. Roberts, R.J. Lillis and M. Manga. 'Giant impacts on early Mars and the cessation of the Martian dynamo'. In: *Journal of Geophysical Research (Planets)* 114.E4, E04009 (Apr. 2009), E04009. DOI: 10.1029/2008JE003287.

[8] Jafar Arkani-Hamed and Peter Olson. 'Giant impacts, core stratification, and failure of the Martian dynamo'. In: *Journal of Geophysical Research (Planets)* 115.E7, E07012 (July 2010), E07012. DOI: 10.1029/2010JE003579.

[9] Constantin Sandu and Walter S. Kiefer. 'Degassing history of Mars and the lifespan of its magnetic dynamo'. In: *Geophysical Research Letters* 39.3 (2012). DOI: https://doi.org/10.1029/2011GL050225. eprint: https://agupubs.onlinelibrary.wiley.com/doi/pdf/10.1029/2011GL050225. URL: https://agupubs.onlinelibrary.wiley.com/doi/abs/10.1029/2011GL050225.

[10] W.H. Press and D.N. Spergel. 'Capture by the sun of a galactic population of weakly interacting, massive particles'. In: *ApJ* 296 (Sept. 1985), pp. 679–684. DOI: 10.1086/163485.

[11] Andrew Gould. 'Resonant Enhancements in Weakly Interacting Massive Particle Capture by the Earth'. In: *The Astrophysical Journal* 321 (Oct. 1987), p. 571. DOI: 10.1086/165653.

[12] Samar Abbas and Afsar Abbas. 'Volcanogenic dark matter and mass extinctions'. In: *Astroparticle Physics* 8.4 (Apr. 1998), pp. 317–320. ISSN: 0927-6505. DOI: 10.1016/s0927-6505(97)00051-0. URL: http://dx.doi.org/10.1016/S0927-6505(97)00051-0.

[13] Michael R. Rampino. 'Disc dark matter in the Galaxy and potential cycles of extraterrestrial impacts, mass extinctions and geological events'. In: *Monthly Notices of the Royal Astronomical Society* 448.2 (Apr. 2015), pp. 1816–1820. DOI: 10.1093/mnras/stu2708.

[14] Rebecca K. Leane and Juri Smirnov. 'Exoplanets as Sub-GeV Dark Matter Detectors'. In: *Physical Review Letters* 126.16 (Apr. 2021). ISSN: 1079-7114. DOI: 10.1103/physrevlett.126.161101. URL: http://dx.doi.org/10.1103/PhysRevLett.126.161101.

[15] D.Bolles. *Dark Energy, Dark Matter.* 2022. URL: https://science.nasa.gov/astrophysics/focus-areas/what-is-dark-energy.

[16] Miguel Zumalacarregui and Uroifmmode Seljak. 'Limits on Stellar-Mass Compact Objects as Dark Matter from Gravitational Lensing of Type Ia Supernovae'. In: *Phys. Rev. Lett.* 121 (14 Oct. 2018), p. 141101. DOI: 10.1103/PhysRevLett.121.141101. URL: https://link.aps.org/doi/10.1103/PhysRevLett.121.141101.

[17] F. Zwicky. 'Republication of: The redshift of extragalactic nebulae'. In: *General Relativity and Gravitation* 41.1 (Jan. 2009), pp. 207–224. DOI: 10.1007/s10714-008-0707-4.

[18] Federico Lelli, Stacy S. McGaugh and James M. Schombert. 'SPARC: Mass Models for 175 Disk Galaxies with Spitzer Photometry and Accurate Rotation Curves'. In: *Astronomical Journal* 152.6, 157 (Dec. 2016), p. 157. DOI: 10.3847/0004-6256/152/6/157. arXiv: 1606.09251 [astro-ph.GA].

[19] Horace W. Babcock. 'The rotation of the Andromeda Nebula'. In: *Lick Observatory Bulletin* 498 (Jan. 1939), pp. 41–51. DOI: 10.5479/ADS/bib/1939LicOB.19.41B.

[20] Leon V. E. Koopmans and Tommaso Treu. 'The Structure and Dynamics of Luminous and Dark Matter in the Early-Type Lens Galaxy of 0047-281 at z = 0.485'. In: *The Astrophysical Journal* 583.2 (Feb. 2003), pp. 606–615. DOI: 10.1086/345423. URL: https://doi.org/10.1086%2F345423.

[21] Henk Hoekstra, H.K.C Yee and Michael D Gladders. 'Current status of weak gravitational lensing'. In: *New Astronomy Reviews* 46.12 (Nov. 2002), pp. 767–781. DOI: 10.1016/s1387-6473(02)00245-2. URL: https://doi.org/10.1016%2Fs1387-6473%2802%2900245-2.

[22] R. Benton Metcalf et al. 'Spectroscopic Gravitational Lensing and Limits on the Dark Matter Substructure in Q2237+0305'. In: *The Astrophysical Journal* 607.1 (May 2004), pp. 43–59. DOI: 10.1086/383243. URL: https://doi.org/10.1086%2F383243.

[23] L. A. Moustakas and R. B. Metcalf. 'Detecting dark matter substructure spectroscopically in strong gravitational lenses'. In: *Monthly Notices of the Royal Astronomical Society* 339.3 (Mar. 2003), pp. 607–615. DOI: 10.1046/j.1365-8711.2003.06055.x. URL: https://doi.org/10.1046%2Fj.1365-8711.2003.06055.x.

[24] John N. Bahcall, Chris Flynn and Andrew Gould. 'Local Dark Matter from a Carefully Selected Sample'. In: *The Astrophysical Journal* 389 (Apr. 1992), p. 234. DOI: 10.1086/171201.

[25] P.J.E. Peebles. 'Large-scale background temperature and mass fluctuations due to scale-invariant primeval perturbations'. In: *The Astrophysical Journal* 263 (Dec. 1982), pp. L1–L5. DOI: 10.1086/183911.

[26] Gianfranco Bertone, Dan Hooper and Joseph Silk. 'Particle dark matter: evidence, candidates and constraints'. In: *Physics Reports* 405.5-6 (Jan. 2005), pp. 279–390. DOI: 10.1016/j.physrep.2004.08.031. URL: https://doi.org/10.1016%2Fj.physrep.2004.08.031.

[27] Leszek Roszkowski, Enrico Maria Sessolo and Sebastian Trojanowski. 'WIMP dark matter candidates and searches: current status and future prospects'. In: *Reports on Progress in Physics* 81.6 (May 2018), p. 066201. DOI: 10.1088/1361-6633/aab913. URL: https://doi.org/10.1088%2F1361-6633%2Faab913.

[28] Lars Bergström. 'Non-baryonic dark matter: observational evidence and detection methods'. In: *Reports on Progress in Physics* 63.5 (Apr. 2000), pp. 793–841. DOI: 10.1088/0034-4885/63/5/2r3. URL: https://doi.org/10.1088%2F0034-4885%2F63%2F5%2F2r3.

[29] Lars Bergström. 'Dark matter candidates'. In: *New Journal of Physics* 11.10 (Oct. 2009), p. 105006. DOI: 10.1088/1367-2630/11/10/105006. URL: https://doi.org/10.1088%2F1367-2630%2F11%2F10%2F105006.

[30] N.T.Tillman. *What is Dark Matter?* 2022. URL: https://www.space.com/20930-dark-matter.html.

[31] Howard Baer et al. 'Dark matter production in the early Universe: Beyond the thermal WIMP paradigm'. In: *Physics Reports* 555 (Feb. 2015), pp. 1–60. DOI: 10.1016/j.physrep.2014.10.002. URL: https://doi.org/10.1016%2Fj.physrep.2014.10.002.

[32] Teresa Marrodan Undagoitia and Ludwig Rauch. 'Dark matter direct-detection experiments'. In: *Journal of Physics G: Nuclear and Particle Physics* 43.1 (Dec. 2015), p. 013001. DOI: 10.1088/0954-3899/43/1/013001. URL: https://doi.org/10.1088%2F0954-3899%2F43%2F1%2F013001.

[33] T. Aralis et al. 'Constraints on dark photons and axionlike particles from the SuperCDMS Soudan experiment'. In: *Phys. Rev. D* 101 (5 Mar. 2020), p. 052008. DOI: 10.1103/PhysRevD.101.052008. URL: https://link.aps.org/doi/10.1103/PhysRevD.101.052008.

[34] Q. Arnaud et al. 'First Germanium-Based Constraints on Sub-MeV Dark Matter with the EDELWEISS Experiment'. In: *Physical Review Letters* 125.14 (Oct. 2020). ISSN: 1079-7114. DOI: 10.1103/physrevlett.125.141301. URL: http://dx.doi.org/10.1103/PhysRevLett.125.141301.

[35] Javier Coronado-Blázquez et al. 'Sensitivity of the Cherenkov Telescope Array to dark subhalos'. In: *Physics of the Dark Universe* 32 (May 2021), p. 100845. ISSN: 2212-6864. DOI: 10.1016/j.dark.2021.100845. URL: http://dx.doi.org/10.1016/j.dark.2021.100845.

[36] The IceCube Collaboration et al. *Search for neutrino lines from dark matter annihilation and decay with IceCube*. 2023. arXiv: 2303.13663 [astro-ph.HE].

[37] Emma Tolley. 'Dark Matter searches with Mono-X signatures at the ATLAS experiment'. In: *PoS* DIS2016 (2016), p. 107. DOI: "10.22323/1.265.0107.

[38] Julio F. Navarro, Carlos S. Frenk and Simon D. M. White. 'The Structure of Cold Dark Matter Halos'. In: *The Astrophysical Journal* 462 (May 1996), p. 563. DOI: 10.1086/177173. URL: https://doi.org/10.1086%2F177173.

[39] J. S. B. Wyithe, E. L. Turner and D. N. Spergel. 'Gravitational Lens Statistics for Generalized NFW Profiles: Parameter Degeneracy and Implications for Self-Interacting Cold Dark Matter'. In: *The Astrophysical Journal* 555.1 (July 2001), p. 504. DOI: 10.1086/321437. URL: https://dx.doi.org/10.1086/321437.

[40] B. Moore et al. 'Cold collapse and the core catastrophe'. In: *Monthly Notices of the Royal Astronomical Society* 310.4 (Dec. 1999), pp. 1147–1152. DOI: 10.1046/j.1365-8711.1999.03039.x. URL: https://doi.org/10.1046%2Fj.1365-8711.1999.03039.x.

[41] A. Burkert. 'The Structure of Dark Matter Halos in Dwarf Galaxies'. In: *The Astrophysical Journal* 447 (July 1995), pp. L25–L28. DOI: 10.1086/309560. arXiv: astro-ph/9504041 [astro-ph].

[42] J. Einasto. 'On the Construction of a Composite Model for the Galaxy and on the Determination of the System of Galactic Parameters'. In: *Trudy Astrofizicheskogo Instituta Alma-Ata* 5 (Jan. 1965), pp. 87–100.

[43] Xiaowei Ou et al. 'The dark matter profile of the Milky Way inferred from its circular velocity curve'. In: *Monthly Notices of the Royal Astronomical Society* 528.1 (Jan. 2024), pp. 693–710. ISSN: 0035-8711. DOI: 10.1093/mnras/stae034. eprint: https://academic.oup.com/mnras/article-pdf/528/1/693/56254192/stae034.pdf. URL: https://doi.org/10.1093/mnras/stae034.

[44] G. Gentile et al. 'The cored distribution of dark matter in spiral galaxies'. In: *Monthly Notices of the Royal Astronomical Society* 351.3 (July 2004), pp. 903–922. ISSN: 0035-8711. DOI: 10.1111/j.1365-2966.2004.07836.x. eprint: https://academic.oup.com/mnras/article-pdf/351/3/903/3595222/351-3-903.pdf. URL: https://doi.org/10.1111/j.1365-2966.2004.07836.x.

[45] Anowar J Shajib et al. 'Dark matter haloes of massive elliptical galaxies at z 0.2 are well described by the Navarro–Frenk–White profile'. In: *Monthly Notices of the Royal Astronomical Society* 503.2 (Feb. 2021), pp. 2380–2405. ISSN: 0035-8711. DOI: 10.1093/mnras/stab536. eprint: https://academic.oup.com/mnras/article-pdf/503/2/2380/36733544/stab536.pdf. URL: https://doi.org/10.1093/mnras/stab536.

[46] Tim Sharp. *How Was Mars Made? | Formation of Mars.* 2017. URL: https://www.space.com/16912-how-was-mars-made.html.

[47] Sean N. Raymond and Alessandro Morbidelli. 'The Grand Tack model: a critical review'. In: *Proceedings of the International Astronomical Union* 9.S310 (July 2014), pp. 194–203. DOI: 10.1017/s1743921314008254. URL: https://doi.org/10.1017%2Fs1743921314008254.

[48] A. Ghosh et al. 'Accretion and Its Effect on the Thermal History of Mars'. In: *Sixth International Conference on Mars* (2003), pp. 1885–.

[49] Angioletta Coradini, Costanzo Federico and Pasquale Lanciano. 'Earth and Mars: early thermal profiles'. In: *Physics of the Earth and Planetary Interiors* 31.2 (1983), pp. 145–160. ISSN: 0031-9201. DOI: https://doi.org/10.1016/0031-9201(83)90106-1. URL: https://www.sciencedirect.com/science/article/pii/0031920183901061.

[50] D. Breuer and W.B. Moore. 'Dynamics and Thermal History of the Terrestrial Planets, the Moon, and Io'. In: *Treatise on Geophysics*. Ed. by Gerald Schubert. 2015, pp. 255–305. DOI: 10.1016/B978-0-444-53802-4.00173-1.

[51] Suzanne E. Smrekar et al. 'Pre-mission InSights on the Interior of Mars'. In: *Scientific Studies of Reading* 215.1, 3 (Jan. 2019), p. 3. DOI: 10.1007/s11214-018-0563-9.

[52] Ana-Catalina Plesa et al. *Interior Dynamics and Thermal Evolution of Mars – a Geodynamic Perspective.* 2022. arXiv: 2207.09283 [astro-ph.EP].

[53] Sam Greenwood, Christopher J. Davies and Anne Pommier. 'Influence of Thermal Stratification on the Structure and Evolution of the Martian Core'. In: *Geophysical Research Letters* 48.22 (2021). e2021GL095198 2021GL095198, e2021GL095198. DOI: https://doi.org/10.1029/2021GL095198. eprint: https://agupubs.onlinelibrary.wiley.com/doi/pdf/10.1029/2021GL095198. URL: https://agupubs.onlinelibrary.wiley.com/doi/abs/10.1029/2021GL095198.

[54] Robert J. Lillis et al. 'Time history of the Martian dynamo from crater magnetic field analysis'. In: *Journal of Geophysical Research (Planets)* 118.7 (July 2013), pp. 1488–1511. DOI: 10.1002/jgre.20105.

[55] *Mars' Crustal Magnetic Field.* Vol. 448. Springer, Cham, 2018, pp. 331–356. DOI: 10.1007/978-3-319-64292-5_12.

[56] 'The history of Mars' dynamo as revealed by modeling magnetic anomalies near Tyrrhenus Mons and Syrtis Major'. In: *Journal of Geophysical Research* 117 (2012). DOI: 10.1029/2012JE004099.

[57] R.J. Lillis et al. 'Unusual magnetic signature of the Hadriaca Patera Volcano: Implications for early Mars'. In: *Geophysical Research Letters* 33.3, L03202 (Feb. 2006), p. L03202. DOI: 10.1029/2005GL024905.

[58] R.J. Lillis, H.V. Frey and M. Manga. 'Rapid decrease in Martian crustal magnetization in the Noachian era: Implications for the dynamo and climate of early Mars'. In: *Geophysical Research Letters* 35.14, L14203 (July 2008), p. L14203. DOI: 10.1029/2008GL034338.

[59] Jean-Pierre Williams and Francis Nimmo. 'Thermal evolution of the Martian core: Implications for an early dynamo'. In: *Geology* 32.2 (Feb. 2004), p. 97. DOI: 10.1130/G19975.1.

[60] David Stevenson. 'Mars' core and magnetism'. In: *Nature* 412 (Aug. 2001), pp. 214–9. DOI: 10.1038/35084155.

[61] M. H. Acuña et al. 'Global Distribution of Crustal Magnetization Discovered by the Mars Global Surveyor MAG/ER Experiment'. In: *Science* 284.5415 (1999), pp. 790–793. DOI: 10.1126/science.284.5415.790. eprint: https://www.science.org/doi/pdf/10.1126/science.284.5415.790. URL: https://www.science.org/doi/abs/10.1126/science.284.5415.790.

[62] James Head et al. 'Geological Processes and Evolution'. In: *Space Science Reviews* 96 (Apr. 2001), pp. 263–292. DOI: 10.1023/A:1011953424736.

[63] Herbert Frey. 'Ages of very large impact basins on Mars: Implications for the late heavy bombardment in the inner solar system'. In: *Geophysical Research Letters* 35.13, L13203 (July 2008), p. L13203. DOI: 10.1029/2008GL033515.

[64] Vincent E. Courtillot. 'A Volcanic Eruption'. In: *Scientific American* 263.4 (1990), pp. 85–93. ISSN: 00368733, 19467087. URL: http://www.jstor.org/stable/24997065 (visited on 03/01/2024).

[65] I. H. Campbell et al. 'Synchronism of the Siberian Traps and the Permian-Triassic Boundary'. In: *Science* 258.5089 (1992), pp. 1760–1763. DOI: 10.1126/science.258.5089.1760. eprint: https://www.science.org/doi/pdf/10.1126/science.258.5089.1760. URL: https://www.science.org/doi/abs/10.1126/science.258.5089.1760.

[66] John J. Matese, Kimmo A. Innanen and Mauri J. Valtonen. 'Variable Oort Cloud Flux due to the Galactic Tide'. In: *Collisional Processes in the Solar System*. Ed. by Mikhail Ya. Marov and Hans Rickman. Dordrecht: Springer Netherlands, 2001, pp. 91–102. ISBN: 978-94-010-0712-2. DOI: 10.1007/978-94-010-0712-2_5. URL: https://doi.org/10.1007/978-94-010-0712-2_5.

[67] P. Nurmi, M.J. Valtonen and J.Q. Zheng. 'Periodic variation of Oort Cloud flux and cometary impacts on the Earth and Jupiter'. In: *Monthly Notices of the Royal Astronomical Society* 327.4 (Nov. 2001), pp. 1367–1376. ISSN: 0035-8711. DOI: 10.1046/j.1365-8711.2001.04854.x. eprint: https://academic.oup.com/mnras/article-pdf/327/4/1367/3284241/327-4-1367.pdf. URL: https://doi.org/10.1046/j.1365-8711.2001.04854.x.

[68] Lisa Randall and Matthew Reece. 'Dark Matter as a Trigger for Periodic Comet Impacts'. In: *Phys. Rev. Lett.* 112 (16 Apr. 2014), p. 161301. DOI: 10.1103/PhysRevLett.112.161301. URL: https://link.aps.org/doi/10.1103/PhysRevLett.112.161301.

[69] Lawrence M. Krauss, Mark Srednicki and Frank Wilczek. 'Solar System constraints and signatures for dark-matter candidates'. In: *Phys. Rev. D* 33 (8 Apr. 1986), pp. 2079–2083. DOI: 10.1103/PhysRevD.33.2079. URL: https://link.aps.org/doi/10.1103/PhysRevD.33.2079.

[70] Raghuveer Garani and Sergio Palomares-Ruiz. 'Dark matter in the Sun: scattering off electrons vs nucleons'. In: *Journal of Cosmology and Astroparticle Physics* 2017.05 (May 2017), pp. 007–007. ISSN: 1475-7516. DOI: 10.1088/1475-7516/2017/05/007. URL: http://dx.doi.org/10.1088/1475-7516/2017/05/007.

[71] Dr. David.R.Williams. *Mars/Earth Comparison.* 2024. URL: https://nssdc.gsfc.nasa.gov/planetary/factsheet/marsfact.html.

[72] Cosmin Ilie, Jacob Pilawa and Saiyang Zhang. 'Comment on "Multiscatter stellar capture of dark matter"'. In: *Phys. Rev. D* 102 (4 Aug. 2020), p. 048301. DOI: 10.1103/PhysRevD.102.048301. URL: https://link.aps.org/doi/10.1103/PhysRevD.102.048301.

[73] Kim Griest and David Seckel. 'Cosmic asymmetry, neutrinos and the sun'. In: *Nuclear Physics B* 283 (Jan. 1987), pp. 681–705. DOI: 10.1016/0550-3213(87)90293-8.

[74] E. Aprile et al. 'Dark Matter Search Results from a One Ton-Year Exposure of XENON1T'. In: *Physical Review Letters* 121.11 (Sept. 2018). ISSN: 1079-7114. DOI: 10.1103/physrevlett.121.111302. URL: http://dx.doi.org/10.1103/PhysRevLett.121.111302.

[75] Joseph Bramante et al. 'Terrestrial and martian heat flow limits on dark matter'. In: *Physical Review D* 101.4 (Feb. 2020). ISSN: 2470-0029. DOI: 10.1103/physrevd.101.043001. URL: http://dx.doi.org/10.1103/PhysRevD.101.043001.

[76] Laura Parro et al. 'Present-day heat flow model of Mars'. In: *Scientific Reports* 7 (Apr. 2017). DOI: 10.1038/srep45629.

[77] Miguel Pato, Fabio Iocco and Gianfranco Bertone. 'Dynamical constraints on the dark matter distribution in the Milky Way'. In: *Journal of Cosmology and Astroparticle Physics* 2015.12 (Dec. 2015), pp. 001–001. ISSN: 1475-7516. DOI: 10.1088/1475-7516/2015/12/001. URL: http://dx.doi.org/10.1088/1475-7516/2015/12/001.

[78] John J. Matese, Kimmo A. Innanen and Mauri J. Valtonen. 'Variable Oort Cloud Flux due to the Galactic Tide'. In: *Collisional Processes in the Solar System.* Ed. by Mikhail Ya. Marov and Hans Rickman. Dordrecht: Springer Netherlands, 2001, pp. 91–102. ISBN: 978-94-010-0712-2. DOI: 10.1007/978-94-010-0712-2_5. URL: https://doi.org/10.1007/978-94-010-0712-2_5.

[79] Julia M. Comerford and Priyamvada Natarajan. 'The observed concentration-mass relation for galaxy clusters'. In: *Monthly Notices of the Royal Astronomical Society* 379.1 (July 2007), pp. 190–200. DOI: 10.1111/j.1365-2966.2007.11934.x. arXiv: astro-ph/0703126 [astro-ph].

[80] Jiao, Yongjun et al. 'Detection of the Keplerian decline in the Milky Way rotation curve'. In: *A&A* 678 (2023), A208. DOI: 10.1051/0004-6361/202347513. URL: https://doi.org/10.1051/0004-6361/202347513.

[81] M. Sten Delos et al. 'Are ultracompact minihalos really ultracompact?' In: *Physical Review D* 97.4 (Feb. 2018). ISSN: 2470-0029. DOI: 10.1103/physrevd.97.041303. URL: http://dx.doi.org/10.1103/PhysRevD.97.041303.

[82] Tomoaki Ishiyama. 'HIERARCHICAL FORMATION OF DARK MATTER HALOS AND THE FREE STREAMING SCALE'. In: *The Astrophysical Journal* 788.1 (May 2014), p. 27. ISSN: 1538-4357. DOI: 10.1088/0004-637x/788/1/27. URL: http://dx.doi.org/10.1088/0004-637X/788/1/27.

[83] E. Contini, G. De Lucia and S. Borgani. 'Statistics of substructures in dark matter haloes'. In: *Monthly Notices of the Royal Astronomical Society* 420.4 (Mar. 2012), pp. 2978–2989. ISSN: 0035-8711. DOI: 10.1111/j.1365-2966.2011.20149.x. eprint: https://academic.oup.com/mnras/article-pdf/420/4/2978/2938141/mnras0420-2978.pdf. URL: https://doi.org/10.1111/j.1365-2966.2011.20149.x.